J. Fluid Mech. (2009), *vol.* 627, *pp.* 291–322.
doi:10.1017/S0022112009005928 Printed in the United Kingdom

Stability of fluid flow through deformable neo-Hookean tubes

GAURAV AND V. SHANKAR†

Department of Chemical Engineering, Indian Institute of Technology, Kanpur 208 016, India

(Received 30 April 2008 and in revised form 7 January 2009)

The linear stability of fully developed Poiseuille flow of a Newtonian fluid in a deformable neo-Hookean tube is analysed to illustrate the shortcomings of extrapolating the linear elastic model for the tube wall outside its domain of validity of small strains in the solid. We show using asymptotic analyses and numerical solutions that a neo-Hookean description of the solid dramatically alters the stability behaviour of flow in a deformable tube. The flow-induced instability predicted to exist in the creeping-flow limit based on the linear elastic approximation is absent in the neo-Hookean model. In contrast, a new low-wavenumber (denoted by k) instability is predicted in the limit of very low Reynolds number ($Re \ll 1$) with $k \propto Re^{1/2}$ for purely elastic (with ratio of solid to fluid viscosities $\eta_r = 0$) neo-Hookean tubes. The first normal stress discontinuity in the neo-Hookean solid gives rise to a high-wavenumber interfacial instability, which is stabilized by interfacial tension at the fluid–wall interface. Inclusion of dissipation ($\eta_r \neq 0$) in the solid has a stabilizing effect on the low-k instability at low Re, and the critical Re for instability is a sensitive function of η_r. For $Re \gg 1$, both the linear elastic extrapolation and the neo-Hookean model agree qualitatively for the most unstable mode, but show disagreement for other unstable modes in the system. Interestingly, for plane-Couette flow past a deformable solid, the results from the extrapolated linear elastic model and the neo-Hookean model agree very well at any Reynolds number for the most unstable mode when the wall thickness is not small. The results of this study have important implications for experimental investigations aimed at probing instabilities in flow through deformable tubes.

1. Introduction and background

The stability of fluid flow through tubes and channels with soft deformable walls has been extensively studied in the last decade, both theoretically (Kumaran 1995, 1998*a*, *b*, 2003; Davies & Carpenter 1997; LaRose & Grotberg 1997; Shankar & Kumaran 2000, 2001; Hamadiche & Gad-el Hak 2002; Gkanis & Kumar 2003, 2005) and experimentally (Kumaran & Muralikrishnan 2000; Muralikrishnan & Kumaran 2002; Eggert & Kumar 2004). The interest in stability of flow through deformable tubes stems from the ubiquity of such systems in the biological realm (Grotberg & Jensen 2004), and more recently in microfluidic device applications (Squires & Quake 2005). While fully developed Poiseuille flow through rigid tubes is stable at any Reynolds number according to linear stability theory (Drazin & Reid 1981), laminar flow through deformable tubes can become linearly unstable because of

† Email address for correspondence: vshankar@iitk.ac.in

flow-induced instabilities at the fluid–wall interface. Indeed, it has been predicted by Kumaran (1995) that flow in a deformable tube can become unstable to axisymmetric disturbances even in the creeping-flow limit (Reynolds number, $Re = 0$), when the non-dimensional parameter characterizing solid deformability $\Gamma = V\eta/(GR_{tube})$ exceeds an $O(1)$ critical value. Here, G is the shear modulus of the solid, R_{tube} is the tube radius, V is the maximum velocity of the laminar flow and η is the viscosity of the fluid. These predictions are based on an extrapolation of the linear elastic model for solid deformations to finite strains, which is strictly valid only in the limit when the strain in the solid is small compared to unity. However, when instability is predicted, the base-state strain in the solid (proportional to the parameter Γ) is $O(1)$ which is outside the domain of validity of the linear elastic solid. Henceforth, we will refer to results obtained using linear elastic model at finite strains as results from the *'extrapolated linear elastic model'* or from the *'linear elastic approximation'*. In order to overcome the inconsistencies inherent in the linear elastic approximation, Gkanis & Kumar (2003, 2005, 2006) used a frame-invariant neo-Hookean model (Malvern 1969; Holzapfel 2000) that takes into account the nonlinear constitutive relation between stress and deformation in a solid. For this case, they showed that the coupling between base-state and perturbation variables occurs at several places in the governing linear stability equations for the solid and interface conditions, in stark contrast to the linear elastic approximation. The manner in which these additional couplings affect the stability of the flow, however, is system-dependent: For plane-Couette flow past a deformable wall, in the creeping-flow limit, results from both the extrapolated linear elastic and neo-Hookean models agree well at larger values of wall thickness when the Γ required for instability becomes small. In contrast, for free-surface gravity-driven creeping flow down a deformable wall, Gkanis & Kumar (2006) showed many qualitative differences between the two approaches, even at larger values of wall thickness.

For the practically important case of fully developed Poiseuille flow in a deformable tube, however, the consequences of employing a neo-Hookean solid model for analysing the stability of the flow have not been examined thus far. Specifically, which predictions of the extrapolated linear elastic model would survive if the wall is modelled as a neo-Hookean solid? The objective of the present study is to determine whether the nonlinear rheological behaviour of the solid qualitatively alters the stability of Poiseuille flow in a deformable tube modelled as a neo-Hookean solid with dissipative effects. Our results show, remarkably, that the stability characteristics for flow in a deformable tube are very different for the neo-Hookean model. This is in contrast to plane-Couette flow, where both the approaches yield qualitatively similar results for thick solids. In the remainder of this section we provide a brief review of relevant previous work, which will help set the context and emphasize the relation of the present work with the existing literature on this subject.

The first systematic experimental study to explore the instability of laminar flow in a soft deformable tube, to our knowledge, is due to Krindel & Silberberg (1979) (also see Lahav, Eliezer & Silberberg 1973; Silberberg 1987), who fabricated micron-sized tubes in soft polyacrylamide gels (shear modulus $\sim 10^3$ Pa). They found that the deviation of the actual flow rate in a gel-walled tube from the expected laminar-flow value occurs at much lower Re compared to 2000 (the transition Re for flow in a rigid tube), and attributed this to an instability of the laminar flow in the deformable tube. The ratio of actual to theoretical laminar flow rates varied smoothly with Re, in contrast to an abrupt transition in a rigid pipe. The transition velocity of the laminar

flow V_t was found to obey the correlation $V_t \propto (GR_{tube}^2/\eta H)$, where G is the shear modulus of the gel, R_{tube} is the radius of the tube, η is the fluid viscosity and H is the thickness of the gel wall. On the theoretical side, Kumaran, Fredrickson & Pincus (1994) and Kumaran (1995), respectively, analysed the stability of plane-Couette flow past a deformable solid and pipe-Poiseuille flow in a deformable tube, by employing a linear elastic approximation for solid deformation. These studies considered the creeping-flow ($Re = 0$) limit, and showed that the flow becomes unstable when the wall deformability parameter Γ (defined above) exceeds a critical $O(1)$ value. Both plane-Couette flow and pipe-Poiseuille flow exhibited several qualitative similarities in terms of their stability characteristics. Gkanis & Kumar (2003) revisited the plane-Couette flow problem in the creeping-flow limit, but used a neo-Hookean solid model to account for finite deformations in the solid, because the base-state strain in the solid (proportional to Γ) is nominally $O(1)$ when the flow is predicted to be unstable by the extrapolated linear elastic solid model. For large values of (non-dimensional) wall thickness H, both the extrapolated linear elastic and neo-Hookean model predictions agreed well, in part because the critical Γ required for instability decreases as $\Gamma \propto H^{-1}$ in the extrapolated linear elastic model, and it is expected that the predictions of the linear elastic approximation will approach those of neo-Hookean solid for small values of Γ. In addition, the first-normal stress difference in the base state of the deformed neo-Hookean solid gives rise to a short-wave instability, much akin to that found in co-extrusion of viscoelastic liquid layers (Renardy 1988), when Γ exceeds a critical $O(1)$ value. For large values of thickness, the most unstable mode is the flow-induced instability which occurs at finite wavenumbers ($0.1 < k < 5$), while for smaller wall thickness $H \leqslant 1$, the short-wave instability ($k > 5$) occurs first as Γ is increased. Experiments by Kumaran & Muralikrishnan (2000) and Eggert & Kumar (2004) carried out in a parallel-plate geometry confirmed the predictions obtained using the extrapolated linear elastic model (Kumaran *et al.* 1994) because of the large values of H (> 5) used in the experiments.

For the stability of creeping flow in a deformable tube, interestingly, the critical value of Γ required for destabilizing the flow in the creeping-flow limit (obtained by the extrapolated linear elastic model) asymptotes to an $O(1)$ quantity even as $H \gg 1$ (Kumaran 1995). Consequently, there exists no regime (such as $H \gg 1$) in a deformable tube where one can *a priori* expect the extrapolated linear elastic model predictions to be valid. It is therefore possible to envision that the predictions for the stability of flow in a neo-Hookean tube could be very different from that of the extrapolated linear elastic model. Motivated by this observation, we carry out a stability analysis in the $Re = 0$ and $Re \ll 1$ (but non-zero) limits for fully developed flow in a neo-Hookean tube in §§ 3.1 and 3.2, and find drastic differences between the results obtained from the two solid models: The creeping-flow instability in a deformable tube predicted using the extrapolated linear elastic model is absent for the neo-Hookean model. Instead, for a neo-Hookean tube, we predict (in § 3.2) a new class of long-wave unstable modes for small (but non-zero) Re which are stabilized by the dissipation in the solid material, and these new modes are absent in the linear elastic approximation.

The unstable mode from the creeping-flow limit obtained using the extrapolated linear elastic model continues (Kumaran 1998*a*) to larger Re, and the solid deformability parameter $\Gamma \propto Re^{-1/3}$ for the instability to exist at $Re \gg 1$. Physically, this unstable mode corresponds to a class of 'wall modes' (Gill 1965; Drazin & Reid 1981), where the viscous effects in the fluid are confined to an $O(Re^{-1/3})$ 'wall

layer' close to the fluid–wall interface. Asymptotic analysis (Shankar & Kumaran 2001) showed that there are multiple downstream (with positive phase velocity) and upstream travelling (with negative phase velocity) wave solutions, all of which are neutrally stable in the leading-order approximation. These discrete modes represent a type of shear waves in the deformable elastic tube, which is a class of transversely propagating waves in an incompressible elastic solid (Achenbach 1973), whose wave speeds scale as $(G/\rho)^{1/2}$ for finite wavenumbers, and as $(G/\rho)^{1/2}(k^* R_{tube})^{-1}$ when the wavenumbers are small $(k^* R_{tube}) \ll 1$. In this work, we label travelling waves as downstream or upstream, respectively, based on whether their wave speeds are positive or negative. For each downstream travelling wave, there is a first correction which becomes unstable above a critical value of Γ, while the upstream travelling modes were always found to be stable. We show in § 3.4 of this paper that, even in the case of wall mode instability, there are some major differences between the predictions from the two solid models. Alongside, we also address similar questions for the case of plane-Couette flow past a neo-Hookean wall, in order to compare and contrast the two geometries. Such a comparison is of interest because the stability of fluid flow in these two geometries, viz., plane-Couette flow and pipe-Poiseuille flow, have many similarities in rigid channels: both lack the 'critical layer' singularity required for the Tollmein–Schlichting instability, and both are linearly stable at all Re (Drazin & Reid 1981). Even for flow past a deformable wall modelled using the linear elastic approximation, plane-Couette flow (Kumaran *et al.* 1994; Srivatsan & Kumaran 1997) and pipe-Poiseuille flow (Kumaran 1995, 1998*a*) have very similar stability characteristics. Our study shows that, remarkably, the results are qualitatively very different for plane-Couette and pipe-Poiseuille flows when the deformable wall is modelled as a neo-Hookean solid.

Another important body of literature related to the present study has focused on the use of flexible solid surfaces for drag-reduction applications by the delay of transition to turbulence using wall flexibility (Carpenter & Garrad 1985, 1986; Carpenter & Gajjar 1990; Carpenter & Morris 1990; Davies & Carpenter 1997; Gad-el hak 2003). These studies have shown that while wall flexibility can delay the onset of Tollmein–Schlichting waves, it could induce new modes of instability in the system. These new modes arise because of the elastohydrodynamic coupling between fluid flow and the wall deformation, and lead to the propagation of waves at the fluid–solid interface. Such unstable waves are often referred to as a 'flow-induced surface instability' (FISI). The instabilities studied in the present work for flow in a deformable tube are also a type of FISI, since the predicted unstable modes are a consequence of solid deformability, and are absent in rigid-walled tubes.

The rest of this paper is organized as follows. The base state, linearized equations and boundary conditions governing the stability of the flow are developed in § 2. In § 3.1, we address the stability of flow in a deformable tube in the creeping-flow ($Re = 0$) limit. The new class of low-Re, low-k unstable modes are identified using asymptotic and numerical methods in §§ 3.2 and 3.3. The behaviour of these unstable modes at high Re and the effect of dissipation in the solid are addressed in § 3.4. The salient conclusions of the present work are given in § 4.

2. Governing equations

We consider the pressure-driven flow of an incompressible Newtonian fluid of density ρ and viscosity η in a deformable tube as shown in figure 1. The inner and outer radii of tube are R_{tube} and $(1 + H)R_{tube}$, respectively. (We use the non-standard

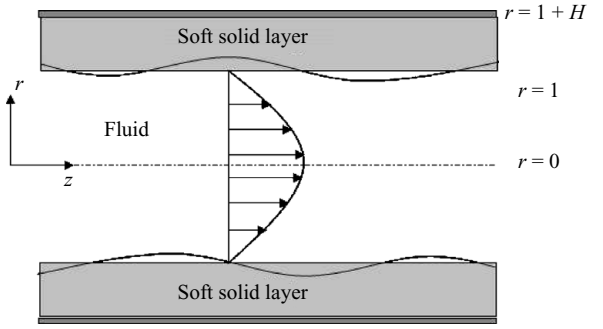

FIGURE 1. Schematic illustration of the configuration and the non-dimensional cylindrical coordinate system: pressure-driven flow of a fluid in a deformable neo-Hookean tube.

notation R_{tube} for tube radius because the symbol R is reserved later for the Lagrangian radial coordinate in the solid.) At the outer surface, the deformable solid is assumed to be perfectly bonded to a rigid tube. The deformable solid of the tube wall is modelled as an impermeable and incompressible neo-Hookean viscoelastic solid (Fosdick & Yu 1996; Hayes & Saccocmandi 2002; Destrade & Saccocmandi 2004) of density ρ, shear modulus G and viscosity η_s. Various physical quantities are non-dimensionalized at the outset by using the following scales: R_{tube} for lengths and deformations, GR_{tube}/η for velocities and G for pressure and stresses. The base flow of interest is the fully developed Hagen–Poiseuille velocity profile

$$\overline{v}_z(r) = \Gamma(1 - r^2), \tag{2.1}$$

where $\Gamma = \eta V/GR_{tube}$ is the non-dimensional maximum velocity in the fluid and V is the dimensional maximum fluid velocity. The non-dimensional governing equations for the fluid are the Navier–Stokes continuity and momentum balance equations

$$\nabla \cdot \boldsymbol{v} = 0, \tag{2.2}$$

$$\frac{Re}{\Gamma}[\partial_t \boldsymbol{v} + \boldsymbol{v} \cdot \nabla \boldsymbol{v}] = -\nabla p + \nabla^2 \boldsymbol{v}. \tag{2.3}$$

where $\boldsymbol{v}$ and p are the velocity and pressure fields in the fluid layer and $Re = \rho V R_{tube}/\eta$ is the Reynolds number based on maximum fluid velocity. In the present scheme of non-dimensionalization (GR_{tube}/η for velocity and η/G for time) the Reynolds number occurs only via the combination $Re/\Gamma = \rho G R_{tube}^2/\eta^2 \equiv \Phi$. Here, Γ measures the strength of the base laminar flow, and Φ characterizes the importance of inertial effects in the fluid and elastic stresses in the solid. Thus, setting $\Phi = 0$ first and keeping Γ arbitrary implies taking the creeping-flow limit, and with non-zero base flow in the tube. Instead, setting $\Gamma = 0$ first and Φ arbitrary would correspond to a static liquid thread inside an elastic tube of varying deformability. If conventional scales (V for velocity, R_{tube}/V for time and R_{tube} for length) are used, this results in Re and Γ being two independent parameters. Under that scheme, Re measures the strength of inertial stresses in the fluid (and solid; see below) and Γ characterizes the ratio of viscous stresses in the fluid to elastic stresses in the solid. If the limit $Re = 0$ is taken first and Γ is kept arbitrary, this corresponds to zero inertia in the fluid and the solid, with base flow velocity being arbitrary. If the $\Gamma = 0$ limit is taken first, this corresponds to a *rigid tube*, with Re measuring the strength of inertial effects with respect to viscous effects.

The governing equations for the fluid are written in terms of spatial (Eulerian) coordinates ($\boldsymbol{x} = r, \theta, z$), while it is convenient (following Gkanis & Kumar 2003) to refer the governing equations for the solid in terms of a reference (Lagrangian) configuration, where the independent variables are the spatial positions $\boldsymbol{X} = (R, \Theta, Z)$ of material particles in the reference (i.e. unstressed) configuration. Thus, the spatial (r, θ, z) coordinate system used for fluid motion is identical to the reference coordinate (R, Θ, Z) system for the deformable solid. In the deformed state of the solid, the spatial positions of the material particles are denoted by $\boldsymbol{w}(\boldsymbol{X})$, where $\boldsymbol{w} = (w_R, w_\Theta, w_Z)$. The deformable solid is modelled as an incompressible neo-Hookean viscoelastic solid and the mass and momentum conservation equations governing the dynamics of solid are given as (Malvern 1969; Holzapfel 2000):

$$\det(\boldsymbol{F}) = 1, \tag{2.4}$$

$$\frac{Re}{\Gamma}\left[\frac{\partial^2 \boldsymbol{w}}{\partial t^2}\right]_{\boldsymbol{X}} = \nabla_{\boldsymbol{X}} \cdot \boldsymbol{P}. \tag{2.5}$$

In the above equations, $\boldsymbol{F}$ is the deformation gradient tensor defined as $\boldsymbol{F} = \nabla_{\boldsymbol{X}} \boldsymbol{w}$ and $\boldsymbol{P}$ is the first Piola–Kirchhoff stress tensor. The first Piola–Kirchhoff stress tensor is related to Cauchy stress tensor by $\boldsymbol{P} = \boldsymbol{F}^{-1} \cdot \boldsymbol{\sigma}$. The Cauchy stress tensor for neo-Hookean viscoelastic solid is split into an elastic part $\boldsymbol{\sigma}_e$ and a dissipative part $\boldsymbol{\sigma}_d$ (Fosdick & Yu 1996; Hayes & Saccocmandi 2002; Destrade & Saccocmandi 2004):

$$\boldsymbol{\sigma} = \boldsymbol{\sigma_e} + \boldsymbol{\sigma_d}, \tag{2.6}$$

$$\boldsymbol{\sigma_e} = -p_s \boldsymbol{I} + \boldsymbol{F} \cdot \boldsymbol{F}^T, \quad \boldsymbol{\sigma_d} = \eta_r (\boldsymbol{L} + \boldsymbol{L}^T). \tag{2.7}$$

where p_s is the pressure-like function related to actual pressure $\hat{p}_s$, in the neo-Hookean solid as $p_s = \hat{p}_s + 1$, $\boldsymbol{L} = \dot{\boldsymbol{F}} \cdot \boldsymbol{F}^{-1}$ is the spatial velocity gradient, overdots represent material time derivatives and $\eta_r = \eta_s/\eta$ is the ratio of solid to fluid viscosity (Chokshi & Kumaran 2007, 2008). To simplify our calculations, we assume a frequency-independent viscosity to describe the dissipative effects in solid medium. Chokshi & Kumaran (2007) have argued that since the velocity of the gel in the base state is zero, it is possible to replace (within a linear stability analysis) the constant viscosity by a frequency-dependent viscosity. Real soft solid materials often exhibit frequency-dependent viscosity (Muralikrishnan & Kumaran 2002; Eggert & Kumar 2004), and the neutral stability curves for such cases can be obtained from a calculation that assumes frequency-independent viscosity by following an iterative procedure described in Muralikrishnan & Kumaran (2002). In the above governing equations for solid layer, the density of the solid is assumed to be equal to the fluid density because the densities of commonly used polymeric gels and elastomers are in general not very different from those of viscous liquids. Thus, the ratio of solid to fluid densities ρ_s/ρ will be close to one, and for small differences in densities we expect that the qualitative predictions of the present study will remain unchanged. However, for $\rho_s/\rho \ll 1$ or $\gg 1$, the density differences could modify the modes explored in the present study and may introduce new modes of instabilities.

The boundary conditions at fluid–solid interface are the continuity of velocities and stresses. At $R = 1 + H$, the deformable solid wall is fixed onto a rigid surface and hence the boundary conditions are those of no deformations ($\boldsymbol{w} = 0$) at the rigid surface. Symmetry conditions ($v_r = 0$ and $d_r v_z = 0$) are used at the tube centre. In the base state, the solid is at rest with a non-zero displacement in z-direction due to shear stress exerted by the base flow in fluid at fluid–solid interface. The overbar in the following equations denote various base-state physical quantities. The steady-state

base deformation and pressure field in solid layer are given as

$$\overline{w}_Z = Z + \Gamma[(1+H)^2 - R^2],\ \overline{w}_R = R, \quad \overline{w}_\Theta = \Theta, \tag{2.8}$$

$$\overline{p}_s = \overline{p}(z) + 4\Gamma^2(R^2-1) - \Sigma, \tag{2.9}$$

where $\Sigma = \gamma / G R_{tube}$ is the non-dimensional interfacial tension parameter at fluid–solid interface and γ is the dimensional interfacial tension. The neo-Hookean solid also exhibits a first normal stress difference in the base state: $\overline{\sigma}_{RR} - \overline{\sigma}_{ZZ} = -4\Gamma^2 R^2$ which results in a short-wave instability (Gkanis & Kumar 2003).

The temporal linear stability of the system is studied by imposing small perturbations to the base state and linearizing the resulting governing equations and boundary conditions about the base-state solution. Only axisymmetric disturbances are considered in the present study, as was done in most of the previous studies. Non-axisymmetric disturbances were analysed by Shankar & Kumaran (2000) for the case of Poiseuille flow in a linear elastic tube, and it was shown that at high Re, the non-axisymmetric modes could be more unstable, while at low and moderate Re axisymmetric disturbances are more unstable. This is because of the possibility of an 'inviscid instability' for flow in a linear elastic tube subjected to non-axisymmetric disturbances. The perturbations to different physical variables are expressed using the standard normal mode decomposition as

$$(v_r', w_R') = (\mathrm{i}\tilde{v}_r(r), \mathrm{i}\tilde{w}_R(R)) \exp[\mathrm{i}k(z-ct)]$$

for normal velocity and normal displacement fluctuations and $f' = \tilde{f}(r)\exp[\mathrm{i}k(z-ct)]$ for fluctuations to all other dynamical variables. Here, f' is the perturbation to any physical variable, $\tilde{f}(r)$ is the complex amplitude function of the disturbance, k is the streamwise wavenumber of perturbations and $c = c_r + \mathrm{i}c_i$ is the complex wave speed. If $c_i > 0$ (or $c_i < 0$), flow will be unstable (or stable). The equations governing the linear stability of the fluid, with $\mathrm{d}_r \equiv \mathrm{d}/\mathrm{d}r$, are

$$\mathrm{d}_r\tilde{v}_r + \frac{1}{r}\tilde{v}_r + k\tilde{v}_z = 0, \tag{2.10}$$

$$-\mathrm{i}k\tilde{p} + \left(\mathrm{d}_r^2 + \frac{1}{r}\mathrm{d}_r - k^2\right)\tilde{v}_z = \mathrm{i}\frac{Re}{\Gamma}[k\tilde{v}_z(\overline{v}_z - c) + \tilde{v}_r \mathrm{d}_r \overline{v}_z], \tag{2.11}$$

$$-\mathrm{d}_r\tilde{p} + \mathrm{i}\left(\mathrm{d}_r^2 + \frac{1}{r}\mathrm{d}_r - \frac{1}{r^2} - k^2\right)\tilde{v}_r = -k\frac{Re}{\Gamma}(\overline{v}_z - c)\tilde{v}_r. \tag{2.12}$$

In the following discussion, the terms enclosed in boxes in the governing equations for deformable solid wall (2.13)–(2.15) and in the interfacial conditions (2.18) and (2.19) represent the different couplings between base state of solid and perturbation variables. These couplings arise due to the constitutive nonlinearities in neo-Hookean solid model, and will be absent if the solid wall is modelled as linear viscoelastic solid. Thus, (2.10)–(2.21) without the boxed terms govern the stability of Hagen–Poiseuille flow in the deformable tube when the solid wall is modelled as linear viscoelastic solid (as in the earlier works of Kumaran 1995, 1998*a*, *b*). The linearized equations for the solid layer are

$$\mathrm{d}_R\tilde{w}_R + \frac{1}{R}\tilde{w}_R + k\tilde{w}_Z + \boxed{2\mathrm{i}k\Gamma R\tilde{w}_R} = 0, \tag{2.13}$$

$$\boxed{-[8\Gamma^2 kR\tilde{w}_R - 4\mathrm{i}\Gamma\left(\mathrm{d}_R + \tfrac{1}{R}\right)\tilde{w}_R]} - \mathrm{i}k\tilde{p}_s + (1 - \mathrm{i}kc\eta_r)\left(\mathrm{d}_R^2 + \frac{1}{R}\mathrm{d}_R - k^2\right)\tilde{w}_Z$$
$$-\boxed{\mathrm{i}kc\eta_r(4\mathrm{i}k\Gamma R\mathrm{d}_R\tilde{w}_Z - 4k^2\Gamma^2R^2\tilde{w}_Z + 4\mathrm{i}k\Gamma\tilde{w}_Z)} = -k^2c^2\frac{Re}{\Gamma}\tilde{w}_Z, \tag{2.14}$$

$$\boxed{[-8\Gamma^2 kR\tilde{w}_Z - 2\Gamma kR\tilde{p}_s + 4\mathrm{i}\Gamma\mathrm{d}_R\tilde{w}_Z]} + \mathrm{i}\mathrm{d}_R\tilde{p}_s + (1 - \mathrm{i}kc\eta_r)\left(\mathrm{d}_R^2 + \frac{1}{R}\mathrm{d}_R - \frac{1}{R^2} - k^2\right)\tilde{w}_R$$
$$-\boxed{\mathrm{i}kc\eta_r(4\mathrm{i}k\Gamma\tilde{w}_R + 4\mathrm{i}k\Gamma R\mathrm{d}_R\tilde{w}_R - 4k^2\Gamma^2R^2\tilde{w}_R)} = -k^2c^2\frac{Re}{\Gamma}\tilde{w}_R. \tag{2.15}$$

The interfacial conditions linearized about the mean fluid–solid interface ($r = 1$) are

$$\tilde{v}_r = -\mathrm{i}kc\,\tilde{w}_R, \tag{2.16}$$
$$\tilde{v}_z + \mathrm{i}\tilde{w}_R\,(\mathrm{d}_r\overline{v}_z)_{r=1} = -\mathrm{i}kc\,\tilde{w}_Z, \tag{2.17}$$
$$\boxed{4\Gamma^2 k\tilde{w}_R - 2\mathrm{i}\Gamma\mathrm{d}_R\tilde{w}_R + 2k^2c\Gamma\eta_r\tilde{w}_Z}$$
$$+(1 - \mathrm{i}kc\eta_r)(\mathrm{d}_R\tilde{w}_Z - k\tilde{w}_R) = (\mathrm{d}_r\tilde{v}_z - k\tilde{v}_r), \tag{2.18}$$
$$\boxed{-8\mathrm{i}\Gamma^2\tilde{w}_R} - \tilde{p}_s + 2\mathrm{i}(1 - \mathrm{i}kc\eta_r)\mathrm{d}_R\tilde{w}_R$$
$$+\boxed{4\mathrm{i}k^2c\eta_r\Gamma\tilde{w}_R} + \Sigma(1 - k^2)\mathrm{i}\tilde{w}_R = -\tilde{p} + 2\mathrm{i}\mathrm{d}_r\tilde{v}_r. \tag{2.19}$$

It must be noted that the term proportional to $\Sigma(1 - k^2)$ in (2.19) contains contributions from both the radial curvature and axial curvature of the liquid–solid interface to linear order. The contribution due to radial curvature (the term Σ), which was neglected in the previous literature (Kumaran 1995, 1998*a*, *b*; Shankar & Kumaran 2000), is responsible for causing a capillary instability similar to the Rayleigh instability of a jet. We show in Appendix A that this destabilizing term could be important in flow through micron-sized deformable tubes.

The symmetry conditions at the tube centre are

$$\tilde{v}_r = 0,\ \ \mathrm{d}_r\tilde{v}_z = 0, \tag{2.20}$$

and finally, the boundary conditions at rigid surface ($R = 1 + H$) are

$$\tilde{w}_R = 0,\ \ \tilde{w}_Z = 0. \tag{2.21}$$

The stability of the system is governed by non-dimensional fluid velocity Γ, Reynolds number Re, viscosity ratio η_r, thickness ratio H and the surface tension parameter Σ. The stability of the system is determined by solving (2.10)–(2.21) for eigenvalue c as a function of k, Re, Γ, H, η_r and Σ. We also discuss the stability characteristics of plane-Couette flow past a neo-Hookean elastic solid at arbitrary Reynolds number in order to compare and contrast the differences in the two geometries. The governing equations for plane-Couette flow past a neo-Hookean solid in the creeping-flow limit are given in Gkanis & Kumar (2003) and Chokshi & Kumaran (2007). These equations are generalized to include fluid and solid inertia in this work, and are not displayed here in the interests of brevity. We employed a combination of asymptotic analyses (in the limits $Re \ll 1$ and $Re \gg 1$) and numerics to investigate the stability characteristics of the present configuration. A pseudo-spectral collocation method (Boyd 1989; Weideman & Reddy 2000) and a numerical shooting procedure (Kumaran 1998*a*; Shankar & Kumaran 2001) with orthonormalization are used to numerically evaluate the eigenvalues and stability boundaries.

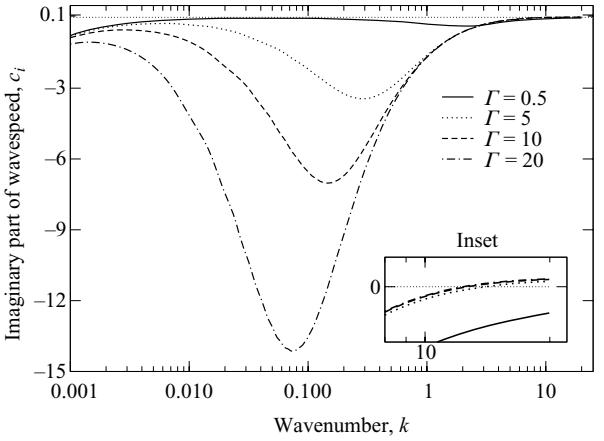

FIGURE 2. c_i vs k curves showing the absence of finite-k viscous mode instability in the creeping-flow limit for a neo-Hookean deformable tube: data for $H = 5$, $Re = 0$ and $\Sigma = 0$. Only the high-k instability is present for $k > 10$, as shown in the inset.

3. Results

In the sections to follow, we show that the use of a neo-Hookean model yields results that are very different from those predicted by extrapolated linear elastic model. We first present the results for a purely elastic neo-Hookean solid with $\eta_r = 0$, and the effect of dissipation in the solid is examined in § 3.4.1.

3.1. *The creeping-flow limit*

We begin by investigating the problem in the absence of inertia, i.e. the creeping-flow limit. This limit is approached by first taking $\Phi \equiv \rho G R_{tube}^2/\eta^2 = Re/\Gamma$ to be zero, and keeping Γ arbitrary. (Instead, if Γ is taken to be zero first, and $\Phi = \rho G R_{tube}^2/\eta^2$ is kept arbitrary, this would represent the case of a static liquid in a deformable tube.) In the absence of flow ($\Gamma = 0$), the only relevant parameters are Σ and solid thickness H. In this no-flow limit, we show in Appendix A that there exists a capillary instability of the liquid inside a soft deformable tube. This capillary instability has been overlooked in the earlier literature (Kumaran 1995, 1998*a*, *b*; Shankar & Kumaran 2000) because of the neglect of the radial curvature of liquid–solid interface in the linearized normal stress balance (2.19). We further show in the Appendix that flow has a stabilizing effect on this instability for a neo-Hookean tube, while it has a destabilizing effect in the extrapolated linear elastic model.

3.1.1. *Flow-induced instability in the creeping-flow limit*

The surface tension-induced instability is shown in Appendix A to be relevant only for micron-sized tubes, and flow has a stabilizing effect on the capillary instability. Thus, we now set $\Sigma = 0$ and focus our attention on the effect of flow (i.e. Γ) on the stability of the system. The characteristic equation is quadratic (in wave speed c) in the creeping-flow limit. One of the two roots for c becomes unstable at high wavenumbers when Γ is increased above a critical value, while the second root remains highly damped at all k for any value of Γ. Figure 2 depicts c_i vs k data for the first root for different values of Γ for a neo-Hookean tube. It is important to mention here that the first root is the same root which exhibits capillary instability for $\Sigma \neq 0$. Figure 2 shows that the short-wave perturbations (with $k \sim 10$) are unstable for higher values of Γ. This short-wave instability is due to the non-zero first normal

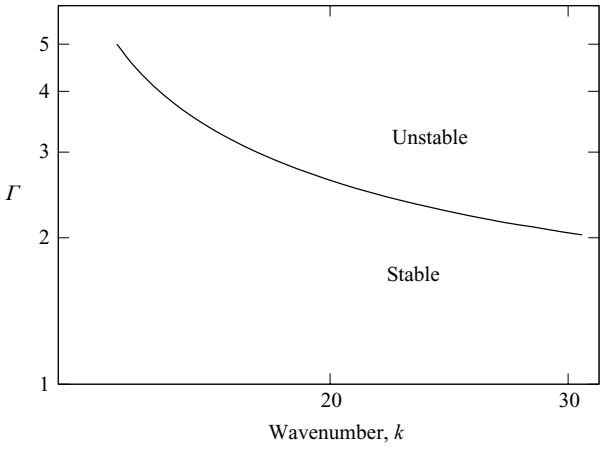

FIGURE 3. Neutral stability curve for the short-wave instability driven by the first normal stress difference in the creeping-flow limit for flow in a neo-Hookean tube: Γ vs k data for $H = 5$, $Re = 0$ and $\Sigma = 0$.

stress difference in base state present for a neo-Hookean solid (Gkanis & Kumar 2003, 2005), and is stabilized by the presence of interfacial tension at the fluid–solid interface. The first normal stress difference in the base state is zero in the linear elastic approximation and thus this high wavenumber instability is absent for flow in the extrapolated linear elastic deformable model. Figure 3 presents the neutral stability data in $\Gamma - k$ plane for $H = 5$ for the normal stress-driven instability. We have verified that the neutral curves for high wavenumber instability remain largely independent of solid thickness. This is because the short-wavelength fluctuations remain localized near the interface and decay rapidly away from the interface. Another important feature to note in figure 2 is that the finite wavenumber (nominally $k \sim O(1)$; practically $0.1 < k < 5$) perturbations do not become unstable for any value of Γ. Figure 2 in fact shows that increase in Γ has a stabilizing effect on finite wavenumber fluctuations for flow through a neo-Hookean tube. In contrast, for the extrapolated linear elastic model (Kumaran 1995), the flow remains stable for lower $\Gamma = 0.1, 0.5$ values and with increase in Γ to $O(1)$ (and higher) the flow becomes unstable for finite wavelength perturbations. The linear elastic approximation does not take into account the effect of finite base-state strain ($\Gamma \sim O(1)$; refer (2.8)) in the solid medium while the neo-Hookean model incorporates the effect of base state of the solid via the different coupling terms between fluctuations and base state present in governing equations of the deformable wall and interfacial conditions. Thus, the more accurate neo-Hookean model predicts that the finite-k instability is absent in a deformable tube in the creeping-flow limit. We have verified using our spectral numerical solution that the finite wavenumber unstable mode is absent for $H \lesssim 100$ and $\Gamma \lesssim 100$.

Indeed, a similar trend was already present in the earlier results of Gkanis & Kumar (2005) for pressure-driven flow in a two-dimensional channel with neo-Hookean walls, where it was shown that the finite-k instability is absent for $H < 10$, while for plane-Couette flow past a neo-Hookean solid, the finite-k instability was present for any H. Thus, pressure-driven flows in a two-dimensional neo-Hookean channel are harder to destabilize compared to plane-Couette flow. The present results show that the stabilizing effect is even more dramatic in the case of pressure-driven flow in a neo-Hookean tube wherein there is no finite-k instability for any value of H in the

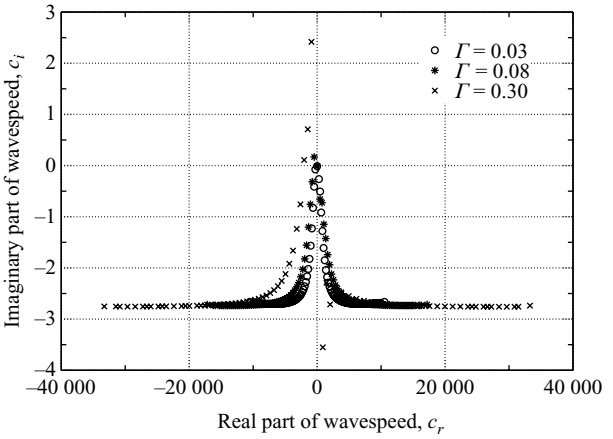

FIGURE 4. Eigenvalue spectrum showing unstable upstream modes at $Re = 0.001$ and $k = 0.01$ for a neo-Hookean tube: data for $H = 9$, $\eta_r = 0$ and $\Sigma = 0$, for different values of Γ.

creeping-flow limit. Thus, in the creeping-flow limit and in the absence of surface tension, the critical mode is the short-wave instability arising because of the first normal stress difference in base state for neo-Hookean solid. To understand the mechanism behind the stabilization in a neo-Hookean tube in the creeping-flow limit, we carry out in Appendix B an analysis similar to the one by Gkanis & Kumar (2003), based on the growth of interfacial fluctuations and various contributions which destabilize or stabilize this growth. It is useful to end this section with an estimate of various parameters for which the short-wave instability could be realized in an experiment. If we consider a deformable tube of radius 10^{-4} m, $V = 0.1$ m s^{-1}, $\eta = 1$ Pa·s, then figure 3 shows that $\Gamma \gtrsim 2$, implying $G \lesssim 500$ Pa in order for the normal stress-induced instability to be realized. Thus, the high-wavenumber instability is expected to be present only in the case of flow of highly viscous liquids in very soft tubes.

3.2. *A new instability at low Re and low wavenumbers*

The short-wave instability discussed above for $Re = 0$ continues to finite Reynolds number and the critical Γ required to destabilize the system remains an $O(1)$ quantity. On the other hand, it was demonstrated in earlier studies using the linear elastic approximation (Shankar & Kumaran 2001) that the finite-k viscous mode is the most unstable mode in creeping-flow limit as well as in low (but non-zero) Re regime. In the present section we investigate the effect of introducing small but finite Re on the stability of flow in a neo-Hookean tube. Specifically, we address the following questions: Will the disturbances with wavelengths other than short waves become unstable in the limit of low Reynolds number? If so, will they alter the critical conditions required to destabilize the system? An important difference between the characteristic equations at $Re = 0$ and $Re \neq 0$ is that for $Re \neq 0$, the characteristic equation admits multiple solutions to c unlike the creeping-flow limit where the characteristic equation was quadratic in c and admits only two solutions for the wave speed. To this end, we used the Chebyshev spectral collocation method (Boyd 1989; Weideman & Reddy 2000) to explore different wavenumber regimes at low Reynolds number.

Figure 4 shows the eigenspectrum for $Re = 0.001$ and $k = 0.01$ at different values of Γ for a neo-Hookean tube. It shows that there are multiple solutions for the eigenvalue

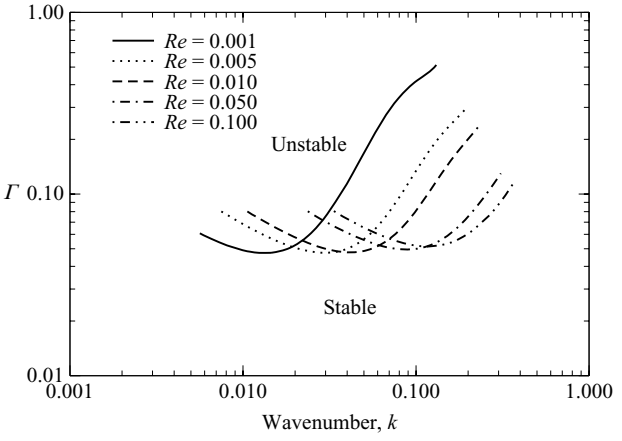

FIGURE 5. Neutral stability data for upstream low-Re, low-k instability in a neo-Hookean tube: Γ vs k for $H = 9$, $\eta_r = 0$, $\Sigma = 0$ and different Re.

c, approximately half of which are downstream travelling waves (eigenvalues with positive real part) and other half are upstream travelling waves (eigenvalues with negative real part). The eigenspectrum in figure 4 shows that for $\Gamma = 0.03$, all eigenmodes are stable. When Γ is increased to 0.08, one of the upstream travelling modes becomes unstable. On further increase in Γ to 0.3, more upstream travelling modes become unstable. It is also observed that the slowest upstream travelling wave (eigenvalue with smallest magnitude of the real part of c) becomes unstable first as the non-dimensional velocity Γ is increased, followed by the upstream wave with next higher wave speed. We adopt the following nomenclature scheme for labelling the modes. The slowest upstream travelling mode is labelled as 'mode-1u' and other upstream modes are designated as 'mode-2u', 'mode-3u etc., in increasing order of their wave speeds. Figure 4 also shows that the downstream modes do not become unstable for any value of Γ. We have verified that this trend persists for different values of Γ and H for low Reynolds number. In fact, as Γ is increased, the downstream modes become further damped indicating the stabilizing effect of Γ on downstream travelling waves. Recall that increase in Γ was also stabilizing for the finite wavenumber viscous mode in the creeping-flow limit, which was also a downstream travelling mode. It is shown later in § 3.4 that downstream travelling modes can become unstable only for $Re \sim O(100)$ or higher. It must be mentioned here that unstable upstream travelling modes were also found in the works of Gkanis & Kumar (2003, 2005, 2006) in the creeping-flow limit for flow in planar geometries.

Figure 5 presents the neutral stability data in Γ–k plane for the first upstream mode (mode-1u) for different Reynolds number. These neutral curves clearly indicate that flow can become unstable for different bands of wavenumbers ranging from $O(0.001)$ to $O(0.1)$ depending on the value of Re. This figure also shows that the neutral stability curves keep shifting towards low-k regime with decrease in Reynolds number. The critical Γ (minimum of a given neutral curve) remains independent of Re while the critical wavenumber 'k_c' decreases with decrease in Reynolds number. We plot the critical conditions (Γ_{crit}, k_c and c_r) as a function of Re (figure 6), and observe that $\Gamma_{crit} \sim O(1)$, $k_c \sim Re^{1/2}$ and wave speed $c_r \sim Re^{-1}$. We have also verified that the Γ–k neutral curves for second upstream mode (mode-2u) show similar qualitative features and identical scalings as mentioned above. These results are in

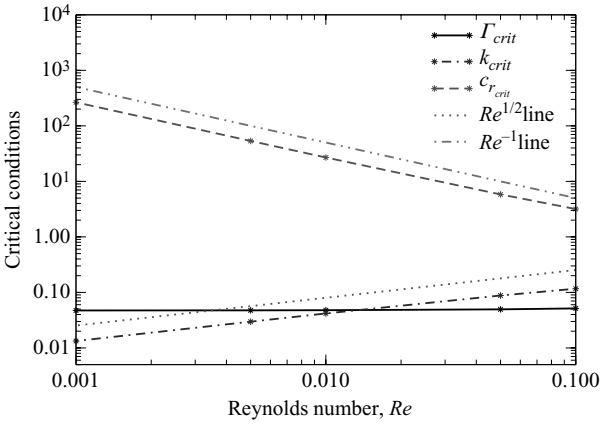

FIGURE 6. Scaling of different variables with Re for the upstream low-Re instability in a neo-Hookean tube: critical conditions as a function of Re for $H = 9$, $\eta_r = 0$ and $\Sigma = 0$.

stark contrast to earlier studies of using the linear elastic approximation where the upstream travelling waves always remain stable for any value of Re and Γ. Thus, this instability of upstream modes for low Re and low wavenumbers must be a consequence of the different couplings between base-state deformation of solid and fluctuations that are present in the governing equations (2.13)–(2.15) and interfacial conditions (2.18) and (2.19) for a neo-Hookean solid model.

It is also of interest here to examine whether the instability is convective or absolute in nature. To this end, the group velocity of the most unstable modes in the spatial stability analysis can be determined from the temporal stability analysis through (Drazin & Reid 1981) $c_g = -\partial(kc_r)/\partial k$, where c_g is the group velocity, and c_r is the real part of the wave speed. We calculated the group velocity of the most unstable mode for the new class of unstable modes and the following trend was observed. When Re is finite, the group velocity is always finite for the most unstable mode, indicating that the instability is of convective nature. However, as $Re \to 0$, the group velocity tends to zero for the most unstable mode, suggesting that the instability could be absolute in nature in this special limit. When Re is finite, the sign of the group speed and phase speeds are same for smaller $Re < 1$, but could be opposite for larger $Re > 1$. Thus, at any finite Re, the instabilities predicted here are expected to be convective in nature.

3.3. *Asymptotic analysis in the limit* $Re \ll 1$, $k \sim Re^{1/2}$

To better understand this new class of multiple unstable modes, we perform an asymptotic analysis in the limit of low Reynolds number to investigate the effect of the different coupling terms in the neo-Hookean tube that could destabilize the upstream travelling waves. The preceding results suggest that $Re^{1/2}$ is a natural candidate for the small parameter of the asymptotic analysis. As mentioned in § 2, the parameter Re always appears through the combination Re/Γ, and we find it convenient to use the small parameter $\epsilon \equiv (Re/\Gamma)^{1/2}$. Since $\Gamma \sim O(1)$, this is equivalent to using $Re^{1/2}$. Based on the numerically obtained scalings shown in figure 6, we assume that $\Gamma \sim O(1)$, $k = k_0\epsilon$ where $k_0 \sim O(1)$ is the scaled non-dimensional wavenumber and the complex wave speed is expanded in a series as

$$c = \frac{1}{\epsilon^2}\left(c^{(0)} + \epsilon c^{(1)} + \cdots\right). \tag{3.1}$$

This scaling of the wave speed $c = c^*/(GR_{tube}/\eta)$ can be verified to be equivalent to the scaling of shear waves in a solid of finite thickness (Achenbach 1973) for which the dimensional wave speed c^* is proportional to $(G/\rho)^{1/2}(k^* R_{tube})^{-1}$, and after noting that for the present class of modes, $k^* R_{tube} \sim \epsilon \ll 1$. We set $\tilde{v}_r \sim O(1)$, thus fluid continuity equation (2.10) and z-momentum equation (2.11) imply $\tilde{v}_z \sim O(\epsilon^{-1})$ and $\tilde{p} \sim O(\epsilon^{-2})$, respectively. Thus, the velocities and pressure in the liquid layer are expanded as

$$\tilde{v}_r = \tilde{v}_r^{(0)} + \epsilon \tilde{v}_r^{(1)} + \epsilon^2 \tilde{v}_r^{(2)} + \cdots, \tag{3.2}$$

$$\tilde{v}_z = \epsilon^{-1}\left(\tilde{v}_z^{(0)} + \epsilon \tilde{v}_z^{(1)} + \epsilon^2 \tilde{v}_z^{(2)} + \cdots\right), \tag{3.3}$$

$$\tilde{p} = \epsilon^{-2}\left(\tilde{p}^{(0)} + \epsilon \tilde{p}^{(1)} + \epsilon^2 \tilde{p}^{(2)} + \cdots\right). \tag{3.4}$$

The normal velocity continuity condition indicates that $\tilde{w}_R \sim O(\epsilon)$ at $r = 1$. We assume that $\tilde{w}_R \sim O(\epsilon)$ in the bulk of the solid as well. Thus, $\tilde{w}_Z \sim O(1)$ and $\tilde{p}_s \sim O(\epsilon^{-1})$ according to the solid continuity equation (2.13) and z-momentum balance (2.13), respectively. The deformation and pressure fields in solid are then expanded as

$$\tilde{w}_R = \epsilon\left(\tilde{w}_R^{(0)} + \epsilon \tilde{w}_R^{(1)} + \cdots\right), \tag{3.5}$$

$$\tilde{w}_Z = \left(\tilde{w}_Z^{(0)} + \epsilon \tilde{w}_Z^{(1)} + \cdots\right), \tag{3.6}$$

$$\tilde{p}_s = \epsilon^{-1}\left(\tilde{p}_s{}^{(0)} + \epsilon \tilde{p}_s{}^{(1)} + \cdots\right). \tag{3.7}$$

The above expansions for the fluid eigenfunctions (3.2)–(3.4), solid eigenfunctions (3.5)–(3.7) and $k = k_0\epsilon$ are substituted in governing equations (2.10)–(2.15) and boundary conditions (2.16)–(2.21) to obtain the set of equations governing the problem at different orders in ϵ. The ordinary differential equation (ODE) governing the leading order $\tilde{v}_r$ is

$$\mathscr{L}_r^2 \tilde{v}_r^{(0)} = 0, \tag{3.8}$$

where $\mathscr{L}_r \equiv (\mathrm{d}_r^2 + r^{-1}\mathrm{d}_r - r^{-2})$. The interfacial conditions ($r = 1$) at leading order $O(\epsilon^0)$ are

$$\tilde{v}_r^{(0)} = -\mathrm{i}k_0 c^{(0)} \tilde{w}_R^{(0)}, \quad \tilde{v}_z^{(0)} = -\mathrm{i}k_0 c^{(0)} \tilde{w}_Z^{(0)}, \quad \mathrm{d}_r \tilde{v}_z^{(0)} = 0, \quad \tilde{p}^{(0)} = 0. \tag{3.9}$$

The conditions at $R = 1 + H$ are simply

$$\tilde{w}_R^{(0)} = 0, \ \tilde{w}_Z^{(0)} = 0 \tag{3.10}$$

and the conditions at tube centre $r = 0$ are finiteness of $\tilde{v}_r^{(0)}$, $\tilde{v}_z^{(0)}$ and $\tilde{p}^{(0)}$. The ODE (3.8) can be solved for $\tilde{v}_r^{(0)}$ as

$$\tilde{v}_r^{(0)} = A_1 r + A_2 r^3 + A_3/r + A_4 \ln r, \tag{3.11}$$

where the constants A_3 and A_4 vanish because of the finiteness of $\tilde{v}_r^{(0)}$ at the centre ($r = 0$) of the tube. While solving for leading-order fluid eigenfunctions, the tangential and normal stress balances (3.9) reduce to $\mathrm{d}_r \tilde{v}_z^{(0)} = -8A_2/k_0$ and $\tilde{p}^{(0)} = 16\mathrm{i}A_2/k_0^2$, respectively. Thus, these two conditions yield the same equation, i.e. $A_2 = 0$. Therefore, the leading-order eigenfunctions for the fluid are

$$\tilde{v}_r^{(0)} = A_1 r, \ \tilde{v}_z^{(0)} = \frac{2A_1}{k_0}, \ \tilde{p}^{(0)} = 0, \tag{3.12}$$

and they are obtained independently of solid layer deformation field. Physically, to leading order, there is a uniform oscillatory perturbation flow in the z-direction. An important point to note is that the leading-order tangential and normal stresses in the

fluid are zero at $r=1$. This is because the stresses in deformable solid wall are $O(\epsilon)$ smaller than the stresses in the fluid. However, the leading-order deformations in the solid are coupled to the leading-order flow in fluid through normal and tangential velocity continuity conditions (3.9). The equations governing the solid at leading order are

$$(\mathrm{d}_R + R^{-1})\tilde{w}_R^{(0)} + k_0\tilde{w}_Z^{(0)} = 0, \tag{3.13}$$

$$-\mathrm{i}k_0\tilde{p}_s^{(0)} + \left(\mathrm{d}_R^2 + R^{-1}\mathrm{d}_R\right)\tilde{w}_Z^{(0)} = -k_0^2 c_0^{(0)^2}\tilde{w}_Z^{(0)}, \tag{3.14}$$

$$\mathrm{d}_R\tilde{p}_s^{(0)} = 0. \tag{3.15}$$

The above set of equations can be solved to give

$$\tilde{w}_R^{(0)} = G_1 R + G_2/R + G_3 J_1\left(k_0 c^{(0)} R\right) + G_4 Y_1\left(k_0 c^{(0)} R\right), \tag{3.16}$$

where J_1 and Y_1 are, respectively, the Bessel functions of first and second kind and G_1, G_2, G_3 and G_4 are constants of integration. The leading-order stress conditions (3.9) and the condition of finiteness of $\tilde{v}_r^{(0)}$ were used to determine constants A_2, A_3 and A_4 while the remaining two velocity continuity conditions (3.9), and zero-displacement conditions (3.10) are still to be used to evaluate the other remaining constants and leading-order wave speed $c^{(0)}$. However, note that we are left with four boundary conditions while we need to evaluate four constants G_1, G_2, G_3 and G_4 (since, A_1 can be arbitrarily specified because the resulting system of equations is linear and homogeneous) along with $c^{(0)}$. Thus, the leading-order conditions are insufficient to determine leading-order wave speed $c^{(0)}$ and it is required to solve for higher order corrections for fluid and solid. The ODE governing the $O(\epsilon)$ correction for the fluid is

$$\mathscr{L}_r^2\tilde{v}_r^{(1)} = 0, \tag{3.17}$$

and the interfacial conditions at $O(\epsilon)$ are

$$\tilde{v}_r^{(1)} = -\mathrm{i}k_0\left(c^{(0)}\tilde{w}_R^{(1)} + c^{(1)}\tilde{w}_R^{(0)}\right), \tag{3.18}$$

$$\tilde{v}_z^{(1)} = -\mathrm{i}k_0\left(c^{(0)}\tilde{w}_Z^{(1)} + c^{(1)}\tilde{w}_Z^{(0)}\right), \tag{3.19}$$

$$\mathrm{d}_r\tilde{v}_z^{(1)} = \mathrm{d}_R\tilde{w}_Z^{(0)}, \tag{3.20}$$

$$\tilde{p}^{(1)} = \tilde{p}_s^{(0)}. \tag{3.21}$$

The solution to the first correction $\tilde{v}_r^{(1)}$ is obtained by solving (3.17) as

$$\tilde{v}_r^{(1)} = A_2 r^3, \quad \tilde{v}_z^{(1)} = -\frac{4A_2}{k_0}r^2. \tag{3.22}$$

Here, in the solution for $\tilde{v}_r^{(1)}$, we have retained only the eigenfunctions that remain finite at $r=0$. There is one more linearly independent solution proportional to r. The constant multiplying this linearly independent solution is set to zero without loss of generality, as this solution is already present at the leading-order solution $\tilde{v}_r^{(0)}$. Equation (3.20) shows that the tangential stress due to first correction in the fluid is balanced by leading-order tangential stress in solid. Similarly, the first correction to fluid pressure is balanced by leading-order pressure in solid (3.21). Recall that the tangential and normal stresses in solid wall do not appear in the leading-order boundary conditions (3.9). This is because the stresses in the solid layer are $O(\epsilon)$ smaller than those in the fluid.

Further analysis reveals that the leading-order wave speed can be determined by substituting the fluid eigenfunctions correct to $O(\epsilon)$ and leading-order solid

eigenfunction in leading-order velocity continuity conditions (3.9), stress continuity conditions at $O(\epsilon)$ (3.20) and (3.21) and (3.10). This results in a system of linear homogeneous equations which can be represented as $\boldsymbol{M}\cdot\boldsymbol{C}^{\boldsymbol{T}}=0$, where $\boldsymbol{C}$ is the vector of constants: $\{A_1, A_2, G_1, G_2, G_3, G_4\}$. The characteristic equation is obtained by setting $\det[\boldsymbol{M}]=0$. There are multiple solutions for $c^{(0)}$ all of which are real, and could be positive or negative. This indicates that in the leading-order approximation, the perturbations are neutrally stable waves travelling in both upstream (with $c^{(0)}$ negative) and downstream directions (with $c^{(0)}$ positive). The various couplings between base-state deformation and fluctuations in the neo-Hookean solid do not appear yet in the calculation of $c^{(0)}$. Thus, the leading-order wave speed will be identical even if one uses the linear elastic model to describe the deformation field in the solid wall. Because the system is neutrally stable up to this level of approximation, it is necessary to calculate the next correction to the wave speed $c^{(1)}$ in order to determine the stability of the system. Subsequent analysis shows that we require the second correction to fluid eigenfunctions and first correction to solid eigenfunctions in order to determine $c^{(1)}$. The ODE governing the second-order correction to fluid velocity field is

$$\mathscr{L}_r\mathscr{L}_r\tilde{v}_r^{(2)} = -\mathrm{i}k_0c^{(0)}\mathscr{L}\tilde{v}_r^{(1)}. \tag{3.23}$$

The solution to the above equation for $\tilde{v}_r^{(2)}$ is obtained as

$$\tilde{v}_r^{(2)} = -\frac{\mathrm{i}k_0c^{(0)}A_2}{24}r^5. \tag{3.24}$$

The equations governing the first correction to the solid eigenfunctions are

$$(\mathrm{d}_R + R^{-1})\tilde{w}_R^{(1)} + k_0\tilde{w}_Z^{(1)} + \boxed{2\mathrm{i}k_0\Gamma R\tilde{w}_R^{(0)}} = 0, \tag{3.25}$$

$$\boxed{4\mathrm{i}\Gamma(\mathrm{d}_R + R^{-1})\tilde{w}_R^{(0)}} - \mathrm{i}k_0\tilde{p}_s{}^{(1)} + \left(\mathrm{d}_R^2 + R^{-1}\mathrm{d}_R\right)\tilde{w}_Z^{(1)} = -k_0^2\left(c^{(0)^2}\tilde{w}_Z^{(1)} + 2c^{(0)}c^{(1)}\tilde{w}_Z^{(0)}\right), \tag{3.26}$$

$$\boxed{-2\Gamma Rk_0\tilde{p}_s^{(0)} + 4\mathrm{i}\Gamma\mathrm{d}_R\tilde{w}_Z^{(0)}} + \mathrm{i}\mathrm{d}_R\tilde{p}_s^{(1)} = 0. \tag{3.27}$$

These are solved to give the following expression for $\tilde{w}_R^{(1)}$:

$$\tilde{w}_R^{(1)} = \left[\frac{2\mathrm{i}\Gamma k_0 + k_0^2c^{(0)}c^{(1)}}{k_0c^{(0)}}\right]\left(G_1RJ_0\left(k_0c^{(0)}R\right) + G_2RY_0\left(k_0c^{(0)}R\right)\right) - G_3\mathrm{i}\Gamma k_0R^3. \tag{3.28}$$

Here, J_0 and Y_0 are, respectively, the Bessel functions of the first and second kind.

Further analysis reveals that the tangential and normal stress conditions at $O(\epsilon^2)$ along with velocity continuity condition for $O(\epsilon)$ at $r=1$ and $\tilde{w}_R^{(1)}=\tilde{w}_Z^{(1)}=0$ at $R=(1+H)$ are required to determine first correction to wave speed. The tangential and normal stress balance at $O(\epsilon^2)$ are

$$\mathrm{d}_r\tilde{v}_z^{(2)} - k_0\tilde{v}_r^{(0)} = \boxed{-2\mathrm{i}\Gamma\mathrm{d}_R\tilde{w}_R^{(0)}} + \mathrm{d}_R\tilde{w}_Z^{(0)}, \tag{3.29}$$

$$\tilde{p}^{(2)} + 2\mathrm{i}\mathrm{d}_r\tilde{v}_r^{(0)} = \tilde{p}_s^{(1)}. \tag{3.30}$$

It is important to mention here that the different coupling terms (terms enclosed in boxes in above equations) due to the neo-Hookean solid appear in the $O(\epsilon)$ correction to solid governing equations (3.25)–(3.27) and in $O(\epsilon^2)$ correction in tangential stress balance (3.29). Thus, it is expected that these couplings will affect the first correction to the wave speed. The coupling due to the first normal stress difference in base state,

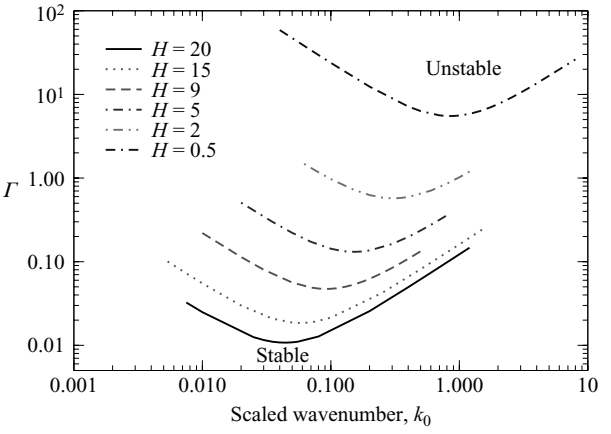

FIGURE 7. Asymptotic results for the unstable upstream mode in neo-Hookean tubes: neutral stability data for mode-1u for different H and $\Sigma = 0$ and $\eta_r = 0$.

which occurs in the tangential stress balance (the term $4\Gamma^2 k\tilde{w}_R$ in (2.18)) and was crucial for the short-wave instability, is however absent in tangential stress condition at $O(\epsilon^2)$ and will not affect the stability of this new class of modes. The solution to the $O(\epsilon^2)$ correction to fluid eigenfunctions and $O(\epsilon)$ correction for solid eigenfunctions are given in (3.24) and (3.28), respectively. These are substituted in the boundary conditions (2.16)–(2.21). As mentioned earlier, the characteristic equation is obtained by setting the $\det[\boldsymbol{M}] = 0$ and this determinant is expanded in a power series in ϵ. The leading-order term of this series yields $c^{(0)}$. The $O(\epsilon)$ correction of determinant is used to evaluate $c^{(1)}$ and it turns out that $c^{(1)}$ is purely imaginary. The flow is stable (unstable) if $c^{(1)} < 0$ ($c^{(1)} > 0$). As already mentioned, that there are multiple solutions for $c^{(0)}$ and these can be either with positive (downstream modes) or negative signs (upstream modes). For each of these $c^{(0)}$, there is a unique first correction $c^{(1)}$ which determines the stability of that mode. The expression for $c^{(1)}$ shows that the upstream travelling waves become unstable when Γ is increased above a critical value for the neo-Hookean solid. The effect of increasing Γ was found to be always stabilizing for the downstream travelling waves. When a linear elastic solid is used, the additional coupling terms (i.e. the terms enclosed in boxes in the above equations) in the solid are absent, and the first correction $c^{(1)}$ is always stable. Thus, the instability of the upstream modes is purely a consequence of the nonlinear neo-Hookean model for the solid.

The condition $c^{(1)} = 0$ can be used to solve for Γ in order to determine the neutrally stable modes. The results for neutral modes obtained from asymptotic analysis were compared with our numerical results and both are found to be in excellent agreement. Recall that the upstream modes were labelled as 'mode-1u','mode-2u' and so on, in increasing order of their wave speeds and the slowest upstream travelling mode is the first one to become unstable as Γ is increased. The asymptotic results also confirm that the first upstream mode is most easily destabilized with increase in base-state velocity. Figure 7 shows neutral curves for mode-1u in $\Gamma - k_0$ plane for different values of H. The critical Γ decreases progressively with increase in solid thickness. Our results show that the critical Γ does not asymptote to a constant value for either $H \gg 1$ or $H \ll 1$. This behaviour is very different from the creeping-flow viscous

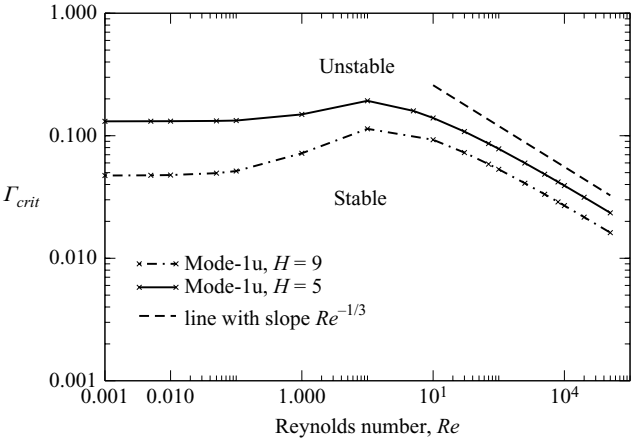

FIGURE 8. Continuation of mode-1u to higher Reynolds number in a neo-Hookean tube for $H = 5$ and $H = 9$.

mode of Kumaran (1995), where the critical Γ asymptotes to a constant $O(1)$ value at $H \ll 1$ and $H \gg 1$. A decrease in critical Γ with H for a neo-Hookean solid, and a plateau for a linear elastic solid, was also seen in the context of free-surface flow down an inclined plane lined with a soft deformable layer by Gkanis & Kumar (2006). We have further verified using our numerical solutions that the scaling assumptions made in the asymptotic analysis for various dynamical variables are consistent with the numerical solution.

The above asymptotic analysis shows that the upstream travelling waves can become unstable in the limit of low Reynolds number for flow through a neo-Hookean tube, but are stable in a linear elastic tube. It is useful to compare the prediction of critical Γ from the two solid models (linear elastic and neo-Hookean) even though the physical nature of unstable modes predicted by two models is entirely different. For example, the linear elastic model predicts the instability of finite wavenumber downstream modes while neo-Hookean solid predicts unstable low-k upstream modes. Kumaran (1995) showed that the $\Gamma_{crit} \to 0.7685$ for $H \gg 1$ and $\Gamma_{crit} \to 4.109$ for $H \ll 1$ for flow through a linear elastic deformable tube in limit of zero Reynolds number. Even for small but finite Reynolds number, previous studies (Shankar & Kumaran 2001) have shown that the critical Γ predicted by using linear elastic model are close to the predictions in the creeping-flow limit, wherein Γ_{crit} approaches an $O(1)$ constant as $H \ll 1$. However, one expects that Γ_{crit} should diverge as $H \to 0$, because one approaches the limit of a rigid wall for $H = 0$. Figure 7 shows that the nonlinear neo-Hookean model correctly recovers this qualitative expectation viz. Γ_{crit} progressively increases with decrease in solid thickness. This prediction is in qualitative agreement with the correlation $\Gamma_{crit} \propto H^{-1}$ reported in the experiments by Krindel & Silberberg (1979).

We end this section with some estimates of the non-dimensional parameters where the low-Re, low-k instability could be realized. For $Re \sim O(1)$, figure 8 shows that $\Gamma_{crit} \sim 0.05$ for $H = 9$. If we set $\eta \sim 10^{-3}$ Pa·s, $R_{tube} \sim 10^{-6}$ m, $V = 1$ m s^{-1}, then $G \sim 2 \times 10^4$ Pa. Instead, if we use a more viscous liquid and a larger tube radius, $\eta = 1$ Pa·s, $R_{tube} \sim 10^{-3}$ m, $V = 1$ m s^{-1}, then $G \sim 2 \times 10^4$ Pa in order for the flow to be unstable. Soft solids with $G \sim 10^4$ Pa can be fabricated using acrylamide or polydimethyl siloxane (PDMS), as has been done in earlier experimental studies

(Kumaran & Muralikrishnan 2000; Eggert & Kumar 2004), and the above predictions can be tested in such systems.

3.4. *Unstable modes at high Re*

In this section, we examine whether the unstable upstream modes analysed above in the low-Re regime continue to intermediate and high Reynolds number. Earlier studies have shown that there exist a set of downstream travelling wall modes which become unstable in the limit of high Reynolds number for flow through linear elastic deformable tubes (Shankar & Kumaran 2001). Here, we explore that whether a similar class of unstable wall modes exist for flow through a neo-Hookean flexible tube, and if they exist, how the stability behaviour of these modes is modified due to the nonlinear rheological behaviour of neo-Hookean solid.

First it is useful here to recall the nature of stability of fluid flow in a rigid tube at high Reynolds number. In the high-Re limit, there are two class of modes in the stability of flow in a rigid tube, wherein the vorticity of the disturbances is confined to thin regions near the centre of the tube or at the wall. The vorticity of the 'centre modes' are confined to a region of thickness of $O(Re^{-1/4})$ near the centre, while the vorticity of the 'wall modes' is confined to a region of thickness $O(Re^{-1/3})$ near the wall. Both these modes are always stable in a rigid tube (Corcos & Sellars 1959; Gill 1965). There have also been many numerical studies (Davey & Drazin 1969; Garg & Rouleau 1972) on the stability of parabolic pipe flow and all these have concluded that the flow is stable to small disturbances at all Reynolds numbers. However, there remains the possibility of non-modal transient algebraic (non-exponential) growth of disturbances for flow in a pipe (which eventually decay exponentially) even within the linear stability theory. During the transient growth phase, small perturbations can be amplified up to a stage where nonlinear effects can become important in the transition to turbulence (Schmid & Henningson 2001).

We first focus our attention on the continuation of upstream unstable travelling modes to high Reynolds number. Figure 8 shows the variation of critical Γ with Re for the first upstream mode for two different values of solid thickness. There are, of course, more unstable upstream modes, but we verified that they show similar qualitative behaviour and thus, the results are shown only for first upstream travelling mode. Moreover, mode-1u is the most unstable mode in the limit of low Reynolds number. The figure shows that the critical Γ remains largely independent of Reynolds number for $Re \ll 1$ which is consistent with the asymptotic results presented in § 3.2. This mode continues to high Reynolds number and Γ decreases as $Re^{-1/3}$ for $Re \gg 1$. The scaling of Γ with Re for these upstream modes is identical to the scaling shown by unstable downstream wall modes in Shankar & Kumaran (2001). We will show a little later that these upstream modes at high Re also correspond to the class of wall modes described in Shankar & Kumaran (2001). For a linear elastic tube, however, the upstream modes do not become unstable for any value Re, H and Γ. Figure 8 also shows that the effect of decreasing H is stabilizing at both low- and high-Re regimes.

Figure 9 shows the eigenspectrum for $H = 9, k = 1$ and $Re = 20\,000$ for different values of Γ. For $\Gamma = 0.001$, all the eigenmodes remain stable. As Γ is increased to 0.005, one of the downstream travelling modes become unstable. With further increase in Γ more downstream travelling modes become unstable and for $\Gamma = 0.05$, both downstream as well as upstream travelling modes become unstable. These unstable modes are numerically continued to both high- and low-Re regime. As mentioned above, the upstream travelling modes continue to the low-k instability

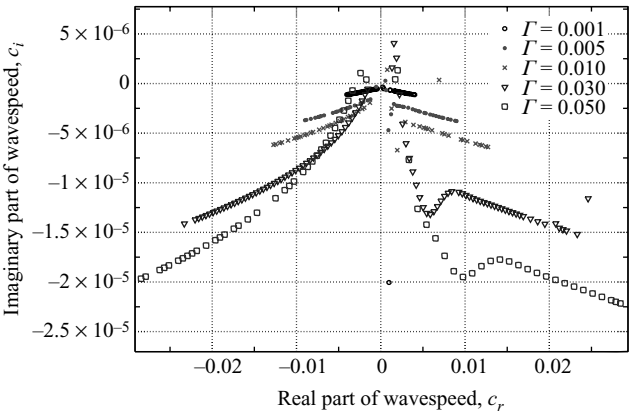

FIGURE 9. Eigenvalue spectrum illustrating different downstream and upstream unstable modes at high Reynolds number in a neo-Hookean tube: data for $H = 9, k = 1, Re = 20\,000$, $\eta_r = 0$ and $\Sigma = 0$.

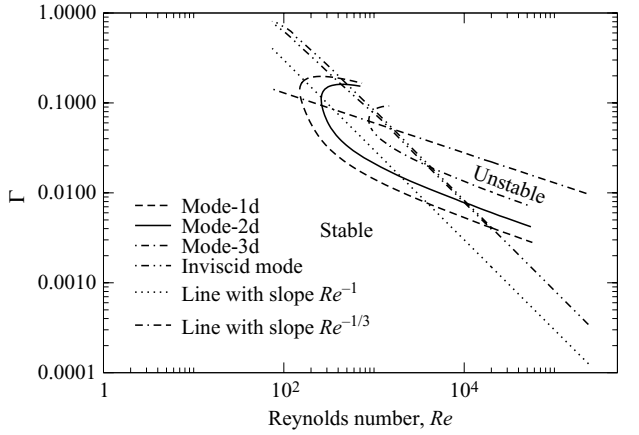

FIGURE 10. Neutral modes showing two different classes of unstable downstream modes with $\Gamma_{crit} \sim Re^{-1/3}$ and $\Gamma_{crit} \sim Re^{-1}$ at high Re in a neo-Hookean tube: data for $H = 9, k = 1, \eta_r = 0$ and $\Sigma = 0$.

in the limit of low Reynolds number (see figure 8). The continuation of unstable downstream modes reveal that there are two different class of modes based on the scaling of Γ with Re in high-Re regime (figure 10). There is one set of unstable downstream travelling modes which shows the scaling behaviour $\Gamma \sim Re^{-1/3}$ while the second set of downstream modes exhibits $\Gamma \sim Re^{-1}$. The latter scaling corresponds to a class of modes termed as 'inviscid modes' (Shankar & Kumaran 2000) where fluid inertial stresses are of the same order as elastic stresses in the solid. We have verified that among these two classes of modes, the first set of downstream modes ($\Gamma \sim Re^{-1/3}$) is most easily destabilized for all Reynolds number ranges of practical interest ($Re < 10^4$). The inviscid mode corresponding to scaling $\Gamma \sim Re^{-1}$ is critical only for $Re \sim O(10\,000)$ or higher. Thus, we focus our attention on the modes for which $\Gamma \sim Re^{-1/3}$. We have further verified that this unstable mode with $\Gamma \sim Re^{-1}$ is present only in a neo-Hookean tube, and is absent in linear elastic tubes.

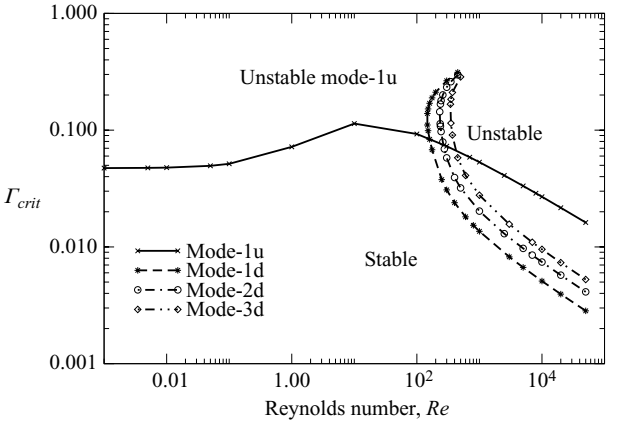

FIGURE 11. Variation of critical Γ with Re for first upstream mode and first three downstream modes in a neo-Hookean tube: data for $H = 9$, $\eta_r = 0$ and $\Sigma = 0$.

Figure 10 shows that there are multiple unstable downstream modes for which $\Gamma \sim Re^{-1/3}$. These modes are labelled as mode-1d, mode-2d, etc., in increasing order of the magnitude of real part of their wave speeds. Thus, mode-1d corresponds to the slowest travelling downstream mode. The scaling $\Gamma \sim Re^{-1/3}$ shown by these downstream and upstream travelling modes in the high-Re limit suggests that these modes correspond to the class of wall modes described in Shankar & Kumaran (2001). To ascertain this, we carried out an asymptotic analysis similar to Shankar & Kumaran (2001) for the case of flow in a neo-Hookean tube, with $Re^{-1/3}$ as a small parameter. Our analysis shows that to leading order, the governing stability equations for the neo-Hookean solid are identical to those for the linear elastic solid, and the wave speed thus determined is therefore identical to the results of Shankar & Kumaran (2001). There are multiple solutions to the leading-order wave speed $c^{(0)}$, all of which are real, but with both positive and negative signs corresponding to downstream and upstream travelling modes. The numerical results for the wave speed corresponding to the neutral data of figures 8 and 10 agree very well with our asymptotic predictions. The asymptotic results for the two solid models, however, differ in the calculation of first correction $c^{(1)}$, because the additional coupling terms (proportional to Γ) in the neo-Hookean solid appear at this order. While only the downstream modes are destabilized in the linear elastic tube, in the neo-Hookean tube, both upstream and downstream modes are destabilized.

Figure 11 shows the variation of critical Γ with Reynolds number for the first three downstream and the first upstream travelling wall modes. It shows that for $Re \gtrsim O(100)$, mode-1d becomes unstable first followed by other downstream and upstream travelling modes. The continuation of downstream modes to lower Reynolds number show that they remain stable below $Re \sim O(100)$. This is in contrast with the earlier results obtained using the extrapolated linear elastic model where all downstream wall modes continue to the low-Re limit and the first downstream mode continues to the creeping-flow viscous mode. Thus, figure 11 shows that for flow through a neo-Hookean deformable tube, the first upstream mode becomes unstable first from $Re \ll 1$ to $Re < 100$, and for $Re \sim O(100)$ and higher, the first downstream wall mode is most easily destabilized. Figure 12 represents the effect of decreasing solid thickness on critical Γ for $Re \sim O(1000)$ for first two downstream wall modes. This shows that for a given Re, the effect of decreasing solid thickness is stabilizing and the

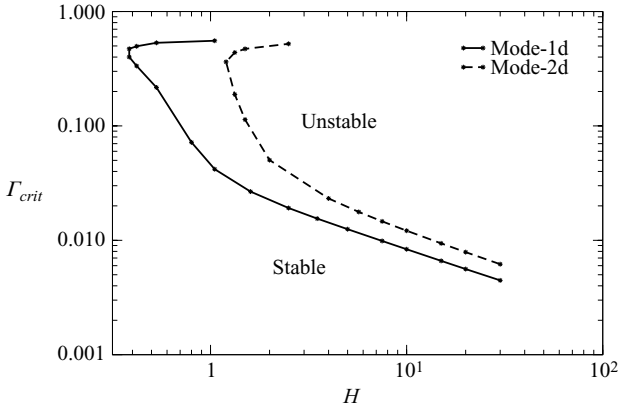

FIGURE 12. Variation of critical Γ with H for the first two downstream modes in a neo-Hookean tube: data for $Re = 2500$, $\eta_r = 0$ and $\Sigma = 0$.

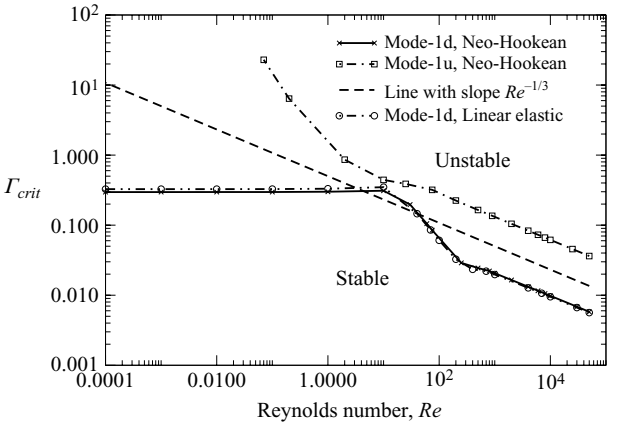

FIGURE 13. Variation of critical Γ with Re for the first upstream mode and downstream modes for plane-Couette flow past a neo-Hookean deformable wall: Γ_{crit} vs Re data for $H = 10$, $\eta_r = 0$ and $\Sigma = 0$. Figure shows that the curve corresponding to downstream mode for the neo-Hookean model agrees very well with the results from the extrapolated linear elastic model. The neutral curve for the upstream mode is absent in the extrapolated linear elastic model.

downstream wall mode instability vanishes for $H \sim O(0.1)$. At higher values of solid thickness, Γ_{crit} decreases with H, in agreement with the experimental observations of Krindel & Silberberg (1979).

It is useful to compare the above results for pipe-Poiseuille flow in a neo-Hookean tube with those for plane-Couette flow past a neo-Hookean wall. The stability characteristics of both these geometries have many similarities in rigid channel. For example, both are linearly stable at all Re and both lack the critical layer singularity required for Tollmein–Schlichting instability. Even for flow past a deformable wall modelled with the linear elastic approximation, these flows have similar stability characteristics (Srivatsan & Kumaran 1997; Kumaran 1998*a*). Figure 13 shows the variation of critical Γ with Re for first upstream and downstream modes for plane-Couette flow past a neo-Hookean deformable solid medium. In the limit of high Re, both upstream and downstream wall modes behave similar to the pipe-Poiseuille flow

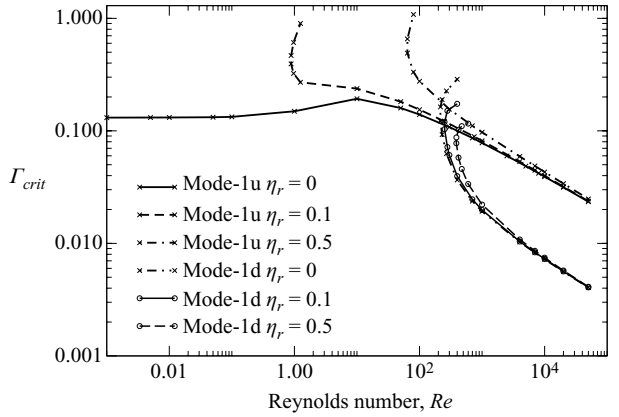

FIGURE 14. Effect of non-zero solid viscosity η_r on the first upstream and downstream modes in a neo-Hookean tube: Γ_{crit} vs Re for $H = 5$ and $\Sigma = 0$.

in deformable tube. For example, $\Gamma \sim O(Re^{-1/3})$ for $Re \gg 1$ and the examination of eigenfunctions in high-Re limit for these two modes reveal that both these modes correspond to the wall modes described in Shankar & Kumaran (2001). However, the continuation of these modes to low-Re limit shows that the stability behaviour of upstream and downstream travelling modes for plane-Couette flow is quite different from pipe-Poiseuille flow. The first downstream mode continues to low-Re limit and $\Gamma \sim O(1)$ while the critical Γ for upstream mode diverges for $Re \ll 1$. On the other hand, for the pipe-Poiseuille case, figure 11 shows that it is the first upstream mode that continues to the low-Re limit, while the downstream modes remain stable for $Re \lesssim O(100)$. Moreover, for $Re = 0$, plane-Couette flow becomes unstable for finite wavenumber perturbations when Γ increases above a critical value unlike pipe-Poiseuille flow where the finite wavenumber fluctuations always remain stable. Figure 13 also shows that, for the most unstable mode, the predictions of both the solid models agree very well at all Reynolds number for plane-Couette flow, in marked contrast with pipe-Poiseuille flow. Our results thus show that while the extrapolated linear elastic model seems adequate to predict instabilities in plane-Couette flow (for solids with $H \gtrsim 1$), for pipe-Poiseuille flow it is imperative to use a nonlinear solid model at any value of solid thickness H.

3.4.1. *Effect of dissipation in the solid*

The results presented thus far are for purely elastic neo-Hookean solid with $\eta_r = 0$. Figures 14 and 15 show the effect of non-zero η_r on the first upstream and downstream modes for $H = 5$ and $H = 9$, respectively. They show the variation of critical Γ with Re at different values of solid viscosity η_r. It can be observed that η_r has little stabilizing effect for both the modes for high Reynolds number. For mode-1d, the critical Reynolds number below which the instability vanishes increases gradually with η_r. However, for mode-1u, the instability in the low-Re limit vanishes rapidly with increase in η_r. For example, when $\eta_r = 0.1$, the instability due to upstream modes disappears for Re below $O(1)$. When solid viscosity is further increased to 0.5, the upstream mode instability is absent for $Re < O(100)$. For non-zero η_r, therefore, the flow through neo-Hookean deformable tubes does not become unstable in the low-Reynolds-number regime and the critical Re above which flow could become unstable increases with η_r. Thus, in the low to moderate Reynolds number regime,

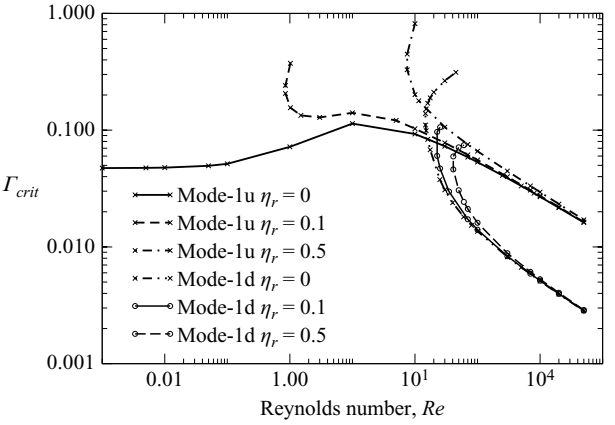

FIGURE 15. Effect of non-zero solid viscosity η_r on the first upstream and downstream modes in a neo-Hookean tube: Γ_{crit} vs Re for $H = 9$ and $\Sigma = 0$.

the critical Reynolds number is expected to be a sensitive function of η_r. The effect of damping in a plate-spring model for a compliant wall has also been addressed in Davies & Carpenter (1997) for pressure-driven flow in a channel. They found very similar stabilization effect of damping on a class of modes termed as 'travelling wave flutter'. However, the travelling wave flutter modes arise in the inviscid limit (of high Re) when there is a critical layer to generate a phase shift between the wall velocity and the perturbation fluid pressure at the wall. For fully developed flow in a pipe analysed in this work, there is no critical layer, and hence the modes analysed here are very different from the travelling wave flutter modes.

3.4.2. *Comparison with Krindel & Silberberg (1979) experiments*

We now attempt to make contact with the earlier experimental results of Krindel & Silberberg (1979) in light of our results. Their experiments used $R_{tube} = 0.15$ mm, $\eta = 10^{-3}$ Pa·s, $H = 8.67$, $G = 320$ Pa. Under these conditions, the transition Reynolds number was experimentally reported to be 570. For this Re, the dimensional velocity can be calculated to be 3.6 m s^{-1}, and hence Γ for their conditions can be estimated to be 0.7. The loss modulus of the solid (which is related to η_r), however, was not reported in their paper. We therefore compare their experimental data with our results for $\eta_r = 0$. From our numerical results for $H = 9$, figure 11 shows that for $Re \sim 600$, the critical Γ required is around 0.015 for $\eta_r = 0$. For non-zero η_r, our numerical results suggest that the critical Γ for instability will increase. Thus, according to our results, the experiments of Krindel & Silberberg (1979) are well in the unstable regime. Krindel & Silberberg (1979) also reported data for a different elastic solid with $G \sim 1200$ Pa. For this solid, the critical Reynolds number was experimentally determined to be 870. The dimensional flow velocity for this Re can be calculated to be 5.4 m s^{-1}, and hence Γ for their experiments can be estimated to be around 0.03. From our numerical results (figure 11), for $Re \sim 900$, the critical Γ for instability is around 0.01. Again, as per our results, the experiments are well in the unstable regime. In addition, our numerical results at low and high Re indicate that Γ_{crit} decreases with increase in H for flow in a neo-Hookean tube, which is in qualitative agreement with the conclusions of Krindel & Silberberg (1979). If a linear elastic model is used (Kumaran 1995), this results in Γ_{crit} being independent of H both for $H \gg 1$ and $H \ll 1$. While this exercise is not aimed at a conclusive quantitative comparison

between our theoretical predictions and observations of Krindel & Silberberg (1979), it certainly suggests a good degree of qualitative agreement between theory and experiments.

4. Conclusions

The stability of Poiseuille flow in a neo-Hookean deformable tube was analysed in different regimes of Reynolds number in order to investigate the implications of using the nonlinear neo-Hookean constitutive relation for the solid on the stability of the flow. In the absence of inertia ($Re = 0$) and flow ($\Gamma = 0$), there exists a capillary instability of the liquid thread inside a soft elastic tube. The effect of flow (by increasing Γ to non-zero values) on the capillary instability was found to be stabilizing for neo-Hookean tubes, and destabilizing for the extrapolated linear elastic model. In the creeping-flow limit and in the absence of interfacial tension, the non-dimensional parameter Γ governs the stability of the system. The neo-Hookean solid exhibits a first normal stress difference in the base state which gives rise to a short-wave instability for $\Gamma \sim O(1)$ or higher. An important result in the creeping-flow limit is the absence of the unstable finite-wavenumber mode for flow through neo-Hookean tubes for any value of Γ and solid thickness H. This is in marked contrast with the prediction of the extrapolated linear elastic model (Kumaran 1995) that creeping flow becomes unstable for finite-wavenumber fluctuations as the velocity increases above a critical value ($\Gamma \sim O(1)$ and higher). The use of a more rigorous neo-Hookean model takes into account the finite base-state strain via the different coupling terms that occur in the linearized governing equations and boundary conditions. These new couplings drastically alter the stability characteristics in the creeping-flow limit for flow in a tube. Interestingly, the predictions from the two models agree for thick solids in the case of a plane-Couette flow.

For low, but finite Re, we predict a new class of multiple upstream travelling modes in a purely elastic neo-Hookean tube which become unstable as Γ is increased above a critical value. These unstable modes are absent in the linear elastic approximation. The critical Γ for these modes remains independent of Re for $Re \ll 1$, but the critical wavenumber scales as $k_c \sim Re^{1/2}$, thus giving rise to a long-wave instability at $Re \ll 1$. These upstream modes continue to the finite- and high-Re regime with $\Gamma \sim O(Re^{-1/3})$ for $Re \gg 1$, and these correspond to the wall modes of Shankar & Kumaran (2001). These upstream travelling modes, however, remain stable for the extrapolated linear elastic model. In the high-Re regime, the neo-Hookean model also predicts multiple unstable downstream travelling wall modes similar to the unstable wall modes predicted in Shankar & Kumaran (2001) using the extrapolated linear elastic model. However, numerical continuation of these downstream modes to lower Re for a neo-Hookean tube revealed that they remain unstable only for $Re > O(100)$. On the other hand, for the extrapolated linear elastic model, the downstream wall modes continue to the creeping-flow limit (Shankar & Kumaran 2001). Upstream travelling modes are found to be critical for the instability in low- and finite-Reynolds-number regime ($Re < O(100)$), while downstream wall modes are critical for $Re \gg 1$. Upon inclusion of dissipation in the solid, the upstream modes are strongly stabilized in the low-Re limit, while there is little effect of η_r on these modes in the high-Re limit.

In conclusion, our study shows that the class of unstable modes of practical interest to the stability of Poiseuille flow to axisymmetric disturbances in a neo-Hookean tube corresponds to shear waves in the elastic tube, which are modified

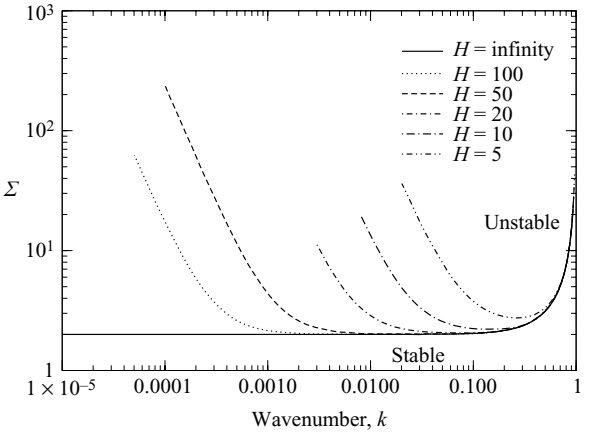

FIGURE 16. Surface-tension-driven instability in an elastic tube in the absence of flow: Σ vs k data for $Re = 0, \Gamma = 0$. Result holds for both extrapolated linear elastic and neo-Hookean solid models.

and destabilized by the fluid flow in different regimes of Reynolds number. Our study also demonstrates that the use of a nonlinear model for the deformable tube not only gives rise to quantitative changes in stability boundaries, but introduces a qualitatively new instability which is absent in the extrapolated linear elastic model and in plane-Couette flow past a deformable solid.

Appendix A. Capillary instability inside a deformable tube

In this appendix, we discuss a capillary-like instability of the liquid inside a deformable tube with and without flow. The characteristic equation is quadratic in the complex wave speed c for $Re = 0$ and $\Gamma = 0$. The liquid–solid interfacial tension Σ is the only parameter which can affect the stability of the system in absence of flow and inertia. One of the two roots of the characteristic equation becomes unstable as Σ increases beyond a critical value while the second root remains highly stable, independent of Σ. This instability of the first root of the characteristic equation is essentially the capillary instability of the stationary liquid thread inside a deformable elastic tube. This instability has been overlooked in the earlier literature (Kumaran 1995, 1998*a*, *b*; Shankar & Kumaran 2000) because of the neglect of the radial curvature of liquid–solid interface in the linearized normal stress balance (2.19). Figure 16 shows the neutral stability diagrams in Σ–k plane for the unstable root for different values of solid thickness. For a given value of solid thickness H, the system becomes unstable when surface tension increases beyond a critical value. As the solid thickness is increased, the critical Σ required to destabilize the system decreases and it asymptotes to a constant value $\Sigma = 2$ for an infinitely thick solid. The neutral stability boundaries shift towards lower wavenumbers with increase in H and for $H \gg 1$, the critical wavenumber approaches to zero. It is important to mention here that for $\Gamma = 0$, the different couplings between perturbation variables and the base state of solid in the governing equations (2.13)–(2.15) and interfacial conditions (2.18) and (2.19) vanish and hence, the linearized stability equations obtained from either of the solid models (neo-Hookean or linear elastic) will be identical. Thus, this surface-tension-driven instability (for $\Gamma = 0$) is independent of whether one uses a nonlinear neo-Hookean model or simple linear elastic approximation.

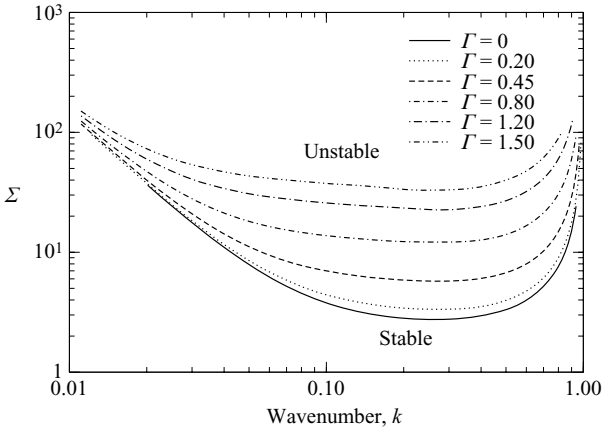

FIGURE 17. Effect of flow in neo-Hookean tube on surface-tension-driven instability: Σ vs k data for $H = 5$ and $Re = 0$.

Figure 17 shows the neutral stability curves (Σ vs k) for $H = 5$ and for different values of Γ for a neo-Hookean tube. Recall that Γ is the non-dimensional maximum velocity in the fluid, and thus, figure 17 shows the effect of flow on the surface-tension-driven instability. The critical Σ required to destabilize the flow increases with Γ, indicating that the flow has a stabilizing effect on capillary instability. Note that for $\Gamma \neq 0$, the neo-Hookean model yields additional coupling terms in the linearized equations when compared with the extrapolated linear elastic solid. Thus, we expect that the effect of introducing flow ($\Gamma \neq 0$) on capillary instability will be different in the two solid models. As mentioned above, the linear elastic approximation will also predict the surface tension-induced instability (identical to the neo-Hookean solid) for $\Gamma = 0$. In contrast, the extrapolated linear elastic model is expected to predict a decrease in critical Σ in presence of flow ($\Gamma \neq 0$), as opposed to the neo-Hookean solid model, for the following reason. It is known that the characteristic equation for the flow in the linear elastic approximation tube is quadratic in c for $Re = 0$ and Γ has destabilizing effect on one of the roots of characteristic equation for finite wavenumber ($k \sim O(1)$) fluctuations (Kumaran 1995). We have verified by gradually increasing Γ to non-zero values (for $\Sigma \neq 0$) that the same root for c exhibits both the capillary and the flow-induced finite wavenumber instability for the extrapolated linear elastic model. Thus, introducing flow has an additional destabilizing effect on the capillary instability and hence the linear elastic approximation predicts a decrease in critical Σ with increase in Γ. This is exactly opposite to the prediction obtained using the neo-Hookean model. We now estimate the parameter regime for which this surface-tension-driven instability can be observed in experiments and real systems. Figure 16 shows that $\Sigma = \sigma/GR_{tube} \sim O(1)$ to trigger the capillary instability. For viscous liquids, $\sigma \sim O(0.1)$ N m^{-1} and if we set $G \sim O(10^4)$ Pa then $\Sigma \sim O(1)$ implies $R_{tube} \sim O(10^{-5})$ m. Thus, the capillary instability will be observed only for micron-sized tubes. This may be of interest in blood flow in small veins and capillaries where the radius is typically of $O(10^{-6})$ m. While our geometry has finite wall thickness, a capillary-like instability in blood vessels modelled as thin elastic membranes induced by the tension in the membrane has been discussed by Alstrom *et al.* (1999).

It is instructive to compare and contrast the capillary instability of a liquid thread inside a deformable elastic tube discussed above with the standard capillary instability

of liquid threads. It is well known that a stationary inviscid or viscous liquid thread suspended in vacuum is linearly unstable for any non-zero value of surface tension for perturbations with $k < 1$ (Rayleigh 1878, 1892). Tomotika (1935) analysed the effect of viscous ambient surroundings in the limit of negligible inertial forces and demonstrated that the instability criterion remains unaltered by the presence of a viscous ambient fluid. While the fluid thread surrounded by an infinite viscous medium is unstable for long waves at any non-zero value of surface tension, the liquid thread bounded by an infinite deformable elastic medium ($H \to \infty$) becomes unstable for $k < 1$ only when surface tension increases beyond a critical value (see figure 16). In order to compare the case of a liquid thread in a deformable tube of finite thickness with a liquid thread surrounded by an external fluid of finite extent, we refer to the core-annular flow (CAF) configuration analysed by Preziosi, Chen & Joseph (1989). Their results illustrate that in absence of inertia, CAF becomes unstable due to capillary forces for $k < 1$ and the critical value of surface tension is zero for CAF as well. On the other hand, figure 16 shows that, for stationary fluid inside a deformable elastic tube of finite H, the fluid–solid interface becomes unstable only for a limited range of wavenumbers when surface tension increases beyond a non-zero critical value. Figure 17 shows that the effect of introducing base-state velocity ($\Gamma \neq 0$) is stabilizing on capillary instability in a neo-Hookean deformable elastic tube. The non-zero base-state velocity implies that there exists an axial shear flow in the fluid which results in an increase of critical Σ required for instability. The stabilizing effect of axial shear flow on capillary instability of a liquid cylinder has also been observed by Russo & Steen (1989). The fluid was set into axial motion by application of an axial shear stress at the free surface. They observed an island of stability for long waves (i.e. partial stabilization in the capillary range) above a critical value of imposed shear stress. A similar stabilization of capillary instability by interfacial shear has been observed by Preziosi *et al.* (1989) for CAF when the less viscous fluid occupies less space and is located near the wall. The capillary forces are always destabilizing for CAF irrespective of the viscosity ratio and the placement of two fluids with respect to the pipe wall. The non-dimensional surface tension parameter in their study was independent of velocity (or rate of shear) and the effect of basic velocity profile was contained in Reynolds number. They showed that for thin less viscous fluid near the wall, stable CAF can be achieved beyond a critical Reynolds number where the capillary instability is stabilized by shear. Thus, the capillary instability of liquid inside a deformable elastic tube is different from capillary instability of liquid threads surrounded by another liquid in two ways: (i) there exists a critical value of surface tension required for instability in the absence of flow and (ii) the effect of flow on the capillary instability is stabilizing in a neo-Hookean tube, while it could be destabilizing or stabilizing in a core-annular liquid system depending on viscosity ratio and thickness ratio of the two liquids.

Appendix B. Mechanism of stabilization in neo-Hookean tubes

To understand the mechanism behind the stabilization in a neo-Hookean tube in the creeping-flow limit, we now carry out an analysis similar to the one by Gkanis & Kumar (2003). We analyse the velocity continuity conditions as this is the only place where time dependence explicitly enters the problem for $Re = 0$

$$v_r{}' = \frac{\partial w_R{}'}{\partial t}, \tag{B 1}$$

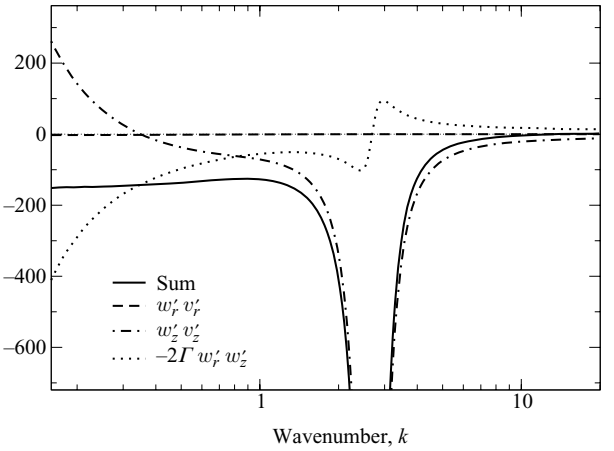

FIGURE 18. The three integrals on the right-hand side of (B 3) for a neo-Hookean solid, and their sum, as a function of wavenumber k. Data for $H=5$, $\Gamma=5$, $Re=0$, $\Sigma=0$. Plot shows that the sum of the integrals is always negative for low and finite wavenumbers. For high wavenumbers, the sum becomes positive because of the high-k instability.

$$v_z' - 2\Gamma w_R' = \frac{\partial w_Z'}{\partial t}, \tag{B 2}$$

where primes denote perturbation variables. Multiplying (B 1) by w_R' and (B 2) by w_Z', adding the resulting equations and averaging over one wavelength of instability yields

$$\frac{1}{2}\frac{\partial}{\partial t}\left[\frac{1}{\lambda}\int_0^\lambda (\boldsymbol{w}'^2)\mathrm{d}Z\right] = \frac{1}{\lambda}\left[\int_0^\lambda w_R' v_r' \mathrm{d}Z + \int_0^\lambda w_Z' v_z' \mathrm{d}Z + \int_0^\lambda \left[-2\Gamma w_R' w_Z' \mathrm{d}Z\right]\right]. \tag{B 3}$$

The left-hand side of (B 3) represents the time rate of change of magnitude of the position of perturbed interface. The right-hand side denotes the various physical contributions which add up to give the rate of change of magnitude of the perturbed interface location. The contribution of a given integral on the right-hand side is stabilizing (destabilizing) if it is negative (positive). The flow is stable (unstable) if sum of the three integrals on the right-hand side is negative (positive). The first integral on the right-hand side represents the interaction of normal velocity and normal interface fluctuations; the second integral represents the interaction of horizontal velocity fluctuation with horizontal interface fluctuation and the third integral represents the effect of mean flow ($-2\Gamma w_R'$) on the horizontal interface deflection.

Figure 18 presents the data for each of the three integrals in (B 3) for $H=5$ and $\Gamma=5$, for a neo-Hookean tube. We first focus our attention on finite wavelength fluctuations ($k \sim O(0.1-10)$). The sum of the three integrals on right-hand side remains negative for $k \sim O(0.1-10)$ indicating that the flow is stable for perturbations corresponding to these wavenumbers, in agreement with the linear stability calculations. The major contribution in the right-hand side comes from the second and third integrals. For lower wavenumbers, the second integral is positive and third is negative, while for $k>1$ the second integral is negative and third is positive. Our numerical calculations show that the sum of second and third integrals is negative

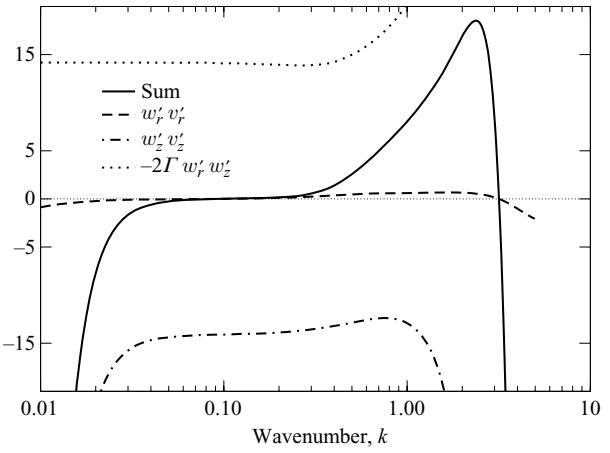

FIGURE 19. The three integrals on the right-hand side of (B 3) for the linear elastic approximation, and their sum, as a function of wavenumber k. Data for $H = 5$, $\Gamma = 5$, $Re = 0$. Plot shows that the sum of the integrals is positive for a band of finite wavenumbers, but is negative at low and high k.

for the wavenumber range mentioned above, and the first integral provides additional negative contribution to balance (B 3). This implies that for low wavenumbers the horizontal velocity perturbations are in phase with horizontal interface fluctuations and thus tend to amplify the disturbance. On the other hand, the mean flow is out of phase with horizontal interface fluctuations and hence tends to suppress them. Thus, for $k < 1$, the stabilizing effect of mean flow overcomes the destabilizing effect of horizontal velocity perturbations on horizontal interface fluctuations. However, these roles are reversed for $k > 1$, i.e. the effect of mean flow on horizontal interface deflection is now destabilizing while the interaction between horizontal interface fluctuation and horizontal velocity perturbation becomes stabilizing and the latter dominates the former. We have verified that the qualitative nature of different integrals on the right-hand side remains similar for different values of H and Γ.

We also performed similar analysis for the extrapolated linear elastic model and observed that the first integral is positive only when flow in the linear approximation is unstable (see figure 19 for $0.1 < k < 3$) while the second integral is always negative and the third integral is always positive. We calculated the sum of second and third integrals and observed that the sum of these two integrals is positive for unstable band of wavenumbers (i.e. $0.1 < k < 3$) while the first integral merely completes the balance in (B 3). This implies that for the extrapolated linear elastic model, the mean flow amplifies the horizontal interface deflection and it dominates the stabilizing effect of horizontal velocity fluctuations on horizontal interface deflection, thus rendering the flow unstable. Based on the above discussion, we conclude that for the case of linear elastic approximation, it is relatively simple to identify the destabilizing mechanism based on the analysis of the velocity continuity conditions. This is possibly because the tangential velocity condition is the only place where time dependence and coupling between mean flow and fluctuations occur for the extrapolated linear elastic model. For flow through a neo-Hookean tube, where the coupling between base state and fluctuations occurs at several places in the linearized equations of the solid, the role of the second and third integrals is rather complicated and depends on the wavenumber

regime. Thus, in contrast to the linear elastic approximation, a simple mechanism cannot be discerned using the above analysis for flow through neo-Hookean tubes.

REFERENCES

Achenbach, J. D. 1973 *Wave Propagation in Elastic Solids*. North-Holland.

Alstrom, P., Eguiluz, V. M., Colding-Jorgensen, M., Gustafsson, F. & Holstein-Rathlou, N-H. 1999 Instability and "sausage-string" appearance in blood vessels during high blood pressure. *Phys. Rev. Lett.* **82**, 1995–1998.

Boyd, J. P. 1989 *Chebyshev and Fourier Spectral Methods*. Springer-Verlag.

Carpenter, P. W. & Gajjar, J. S. B. 1990 A general theory for two and three dimensional wall-mode instabilities in boundary layers over isotropic and anisotropic compliant walls. *Theor. Comput. Fluid Dyn.* **1**, 349–378.

Carpenter, P. W. & Garrad, A. D. 1985 The hydrodynamic stability of flows over Kramer-type compliant surfaces. Part 1. Tollmien--Schlichting instabilities. *J. Fluid Mech.* **155**, 465–510.

Carpenter, P. W. & Garrad, A. D. 1986 The hydrodynamic stability of flows over Kramer-type compliant surfaces. Part 2. Flow induced surface instabilities. *J. Fluid Mech.* **170**, 199–232.

Carpenter, P. W. & Morris, P. J. 1990 The effect of anisotropic wall compliance on boundary-layer stability and transition. *J. Fluid Mech.* **218**, 171–223.

Chokshi, P. & Kumaran, V. 2007 Stability of the flow of a viscoelastic fluid past a deformable surface in the low Reynolds number limit. *Phys. Fluids* **19**, 014103.

Chokshi, P. & Kumaran, V. 2008 Weakly nonlinear analysis of viscous instability in flow past a neo-Hookean surface. *Phys. Rev.* E **77**, 056303.

Corcos, G. M. & Sellars, J. R. 1959 On the stability of fully developed pipe flow. *J. Fluid Mech.* **5**, 97–112.

Davey, A. & Drazin, P. G. 1969 The stability of Poiseuille flow in a pipe. *J. Fluid Mech.* **36**, 209–218.

Davies, C. & Carpenter, P. W. 1997 Instabilities in a plane channel flow between compliant walls. *J. Fluid Mech.* **352**, 205–243.

Destrade, M. & Saccocmandi, G. 2004 Finite–amplitude inhomogeneous waves in Mooney–Rivlin viscoelastic solids. *Wave Motion* **40**, 251–262.

Drazin, P. G. & Reid, W. H. 1981 *Hydrodynamic Stability*. Cambridge University Press.

Eggert, M. D. & Kumar, S. 2004 Observations of instability, hysterisis, and oscillation in low-Reynolds number flow past polymer gels. *J. Colloid Interface Sci.* **274**, 234–242.

Fosdick, R. L. & Yu, J. H. 1996 Thermodynamics, stability and non–linear oscillations of viscoelastic solids – I. Differential type solids of second grade. *Intl J. Non-Linear Mech.* **31**, 495–516.

Gad-el hak, M. 2003 Drag reduction using compliant walls. In *IUTAM Symposium on Flow Past Highly Compliant Boundaries and in Collapsible Tubes* (ed. P. W. Carpenter & T. J. Pedley), chap. 9, pp. 191–229. Kluwer Academic.

Garg, V. K. & Rouleau, W. T. 1972 Linear spatial stability of pipe Poiseuille flow. *J. Fluid Mech.* **36**, 209–218.

Gill, A. E. 1965 On the behaviour of small disturbances to Poiseuille flow in a circular pipe. *J. Fluid Mech.* **21**, 145–172.

Gkanis, V. & Kumar, S. 2003 Instability of creeping Couette flow past a neo-Hookean solid. *Phys. Fluids* **15**, 2864–2471.

Gkanis, V. & Kumar, S. 2005 Stability of pressure-driven creeping flows in channels lined with a nonlinear elastic solid. *J. Fluid Mech.* **524**, 357–375.

Gkanis, V. & Kumar, S. 2006 Instability of gravity-driven free-surface flow past a deformable elastic solid. *Phys. Fluids* **18**, 044103.

Grotberg, J. B. & Jensen, O. E. 2004 Biofluid mechanics in flexible tubes. *Annu. Rev. Fluid Mech.* **36**, 121–147.

Hamadiche, M. & Gad-el Hak, M. 2002 Temporal stability of flow through viscoelastic tubes. *J. Fluids Struct.* **16**, 331–359.

Hayes, M. A. & Saccocmandi, G. 2002 Finite–amplitude waves superimposed on pseudoplanar motions for Mooney–Rivlin viscoelastic solids. *Intl J. Non-Linear Mech.* **37**, 1139–1146.

Holzapfel, G. A. 2000 *Nonlinear Solid Mechanics*. John Wiley.

Krindel, P. & Silberberg, A. 1979 Flow through gel-walled tubes. *J. Colloid Interface Sci.* **71**, 34–50.

Kumaran, V. 1995 Stability of the viscous flow of a fluid through a flexible tube. *J. Fluid Mech.* **294**, 259–281.

Kumaran, V. 1998*a* Stability of fluid flow through a flexible tube at intermediate Reynolds number. *J. Fluid Mech.* **357**, 123–140.

Kumaran, V. 1998*b* Stability of wall modes in a flexible tube. *J. Fluid Mech.* **362**, 1–15.

Kumaran, V. 2003 Hydrodynamic stability of flow through compliant channels and tubes. In *IUTAM Symposium on Flow Past Highly Compliant Boundaries and in Collapsible Tubes* (ed. P. W. Carpenter & T. J. Pedley), chap. 5, pp. 95–118. Kluwer Academic.

Kumaran, V., Fredrickson, G. H. & Pincus, P. 1994 Flow induced instability of the interface between a fluid and a gel at low Reynolds number. *J. Phys. II France* **4**, 893–904.

Kumaran, V. & Muralikrishnan, R. 2000 Spontaneous growth of fluctuations in the viscous flow of a fluid past a soft interface. *Phys. Rev. Lett.* **84**, 3310–3313.

Lahav, J., Eliezer, N. & Silberberg, A. 1973 Gel-walled cylindrical channels as models for micro-circulation: dynamics of flow. *Biorheology* **10**, 595–604.

LaRose, P. G. & Grotberg, J. B. 1997 Flutter and long-wave instabilities in compliant channels conveying developing flows. *J. Fluid Mech.* **331**, 37–58.

Malvern, L. E. 1969 *Introduction to the Mechanics of a Continuous Medium*. Prentice-Hall.

Muralikrishnan, R. & Kumaran, V. 2002 Experimental study of the instability of viscous flow past a flexible surface. *Phys. Fluids* **14**, 775–780.

Preziosi, L., Chen, K. P. & Joseph, D. D. 1989 Lubricated pipelining: stability of core-annular flow. *J. Fluid Mech.* **201**, 323–356.

Rayleigh, L. 1878 On the instability of jets. *Proc. London Math. Soc.* **10**, 4–13.

Rayleigh, L. 1892 On the stability of cylinder of viscous liquid under capillary force. *Phil. Mag.* **34**, 145–154.

Renardy, Y. 1988 Stability of the interface in two-layer Couette flow of upper convected Maxwell liquids. *J. Non-Newtonian Fluid Mech.* **28**, 99–115.

Russo, M. J. & Steen, P. H. 1989 Shear stabilisation of capillary breakup of a cylindrical interface. *Phys. Fluids* A **1**, 1926–1937.

Schmid, P. J. & Henningson, D. S. 2001 *Stability and Transition in Shear Flows*. Springer-Verlag.

Shankar, V. & Kumaran, V. 2000 Stability of fluid flow in a flexible tube to non-axisymmetric disturbances. *J. Fluid Mech.* **408**, 291–314.

Shankar, V. & Kumaran, V. 2001 Asymptotic analysis of wall modes in a flexible tube revisited. *Euro. Phys. J. B.* **19**, 607–622.

Silberberg, A. 1987 Physico-chemical hydrodynamics in turbulent flows close to an interface. *Phys.-Chem. Hydrodyn.* **9**, 419–426.

Squires, T. M. & Quake, S. R. 2005 Microfluidics: fluid physics at the nanoliter scale. *Rev. Mod. Phys.* **77**, 977–1026.

Srivatsan, L. & Kumaran, V. 1997 Stability of the interface between a fluid and gel. *J. Phys. II. France.* **7**, 947–963.

Tomotika, S. 1935 On the instability of cylindrical thread of a viscous liquid surrounded by another viscous fluid. *Proc. R. Soc.* A **150**, 322–337.

Weideman, J. A. C. & Reddy, S. C. 2000 A Matlab differentiation matrix suite. *ACM Trans. Math. Software* **26**, 465–519.